Desulfurization of Model Fuel Oil Using Modified Lignin@S-g-C_3N_4: Optimization *via* Response Surface Methodology

MS Thesis

by

Saba Iqbal

CIIT/SP24-R06-014/LHR

COMSATS University Islamabad

Pakistan

FALL 2025

Desulfurization of Model Fuel Oil Using Modified Lignin@S-g-C_3N_4: Optimization *via* Response Surface Methodology

A thesis submitted to

COMSATS University Islamabad

In partial fulfillment

Of the requirements for the degree of

Master of Science
in
Chemistry

by

Saba Iqbal

CIIT/SP24-R06-014/LHR

Department of Chemistry

Faculty of Chemistry

COMSATS University Islamabad

Pakistan

FALL 2025

Desulfurization of Model Fuel Oil Using Modified Lignin@S-g-C_3N_4: Optimization *via* Response Surface Methodology

This thesis is submitted to the Department of Chemistry in partial fulfillment of the requirements for the award of the degree of Master of Science in Chemistry

Name	Registration Number
Saba Iqbal	CIIT/SP24-R06-014/LHR

Supervisor Committee

Supervisor

Dr. Sadaf Ul Hassan
Assistant Professor
Department of Chemistry
COMSATS University Islamabad
(CUI)
Lahore Campus

Member

Dr. Zulfiqar Ali
Professor
Department of Chemistry
COMSATS University Islamabad
(CUI)
Lahore Campus

Member

Dr. M. Shahid Nazir
Associate Professor
Department of Chemistry
COMSATS University Islamabad
(CUI)
Lahore Campus

Certificate of Approval

This thesis titled

Desulfurization of Model Fuel Oil Using Modified Lignin@S-g-C_3N_4: Optimization *via* Response Surface Methodology

By

Saba Iqbal
CIIT/SP24-R06-014/LHR

has been approved

for the degree of Master of Science in Chemistry
at COMSATS University Islamabad, Lahore Campus

External Examiner: _____

Dr. Abid Ali (Ass. Prof.)
University of Lahore

Supervisor: _____

Dr. Sadaf Ul Hassan (Asst. Prof.)
Department of Chemistry
CUI, Lahore Campus

Head of the Department: _____

Dr. M. Shahid Nazir
Department of Chemistry
CUI, Lahore Campus

Author's Declaration

I Saba Iqbal, CIIT/SP24-R06-0014/LHR, hereby declare that I have produced the work presented in this thesis, during the scheduled period of study. I also declare that I have not taken any material from any source except referred to wherever due to that amount of plagiarism is within an acceptable range. If a violation of HEC rules on research has occurred in this thesis, I shall be liable to punishable action under the plagiarism rules of HEC.

Date: _____

Date of Thesis submission

Signature of Student

_____

Saba Iqbal

CIIT/SP24-R06-014/LHR

Certificate

It is certified that Saba Iqbal, CIIT/SP24-R06-014/LHR, has carried out all the work related to this thesis under my supervision at Department of Chemistry, COMSATS University Islamabad, Lahore Campus and the work fulfil the requirement for the award of the degree of MS in Chemistry.

Date: _____

Date of thesis submission

Supervisor:

Sign

Dr. Sadaf Ul Hassan
Assistant Professor
Department of
Chemistry
COMSATS University
Islamabad Lahore Campus

Dedication

This thesis is respectfully dedicated to my family, especially my mother, whose endless prayers, unconditional love, and sacrifices have been the foundation of every achievement in my life. I am deeply grateful to my esteemed supervisor, Dr. Sadaf Ul Hassan, for his kind guidance, encouragement, and continuous support throughout this research journey, without which this work would not have been possible. I also sincerely acknowledge my brothers for their constant encouragement and support during this journey.

Acknowledgements

All praise and gratitude belong to **Allah Almighty**, the Most Beneficent and the Most Merciful, whose countless blessings, grace, and mercy granted me the strength, guidance, and perseverance to successfully complete this dissertation. I also express my deepest reverence and gratitude to the **Holy Prophet Hazrat Muhammad (SAW),** whose teachings and wisdom continue to illuminate the path for all of humanity.

With profound respect, I extend my sincere gratitude to my esteemed research supervisor, **Dr. Sadaf Ul Hassan**, for her invaluable mentorship, expert guidance, constructive feedback, and continuous encouragement throughout the entire course of this research. Her knowledge, experience, and kind support played a pivotal role in the successful completion of this project. It has been a great honor and privilege to work under the supervision of such a dedicated and inspiring mentor.

I am also sincerely thankful to **Mam Samra Syed** for her generous support in providing the necessary laboratory facilities. Her cooperation, guidance, and assistance during my experimental work are highly appreciated.

I would like to express my heartfelt gratitude to my friend **Hina Murtaza** and all my lab fellows for their unwavering support, encouragement, and companionship throughout this research journey. Your cooperation and shared perseverance during challenging times made this journey both manageable and memorable.

I owe my deepest gratitude to my parents and siblings, whose constant emotional support, prayers, and financial assistance have been the backbone of my academic journey.

Finally, I extend my sincere thanks to the Synthetic Chemistry Laboratory and the Department of Chemistry for providing the resources, facilities, and environment necessary to carry out this research successfully.

Saba Iqbal
CIIT/SP24-R06-014/LHR

Abstract

Desulfurization of Model Fuel Oil Using Modified Lignin@S-g-C_3N_4: Optimization *via* Response Surface Methodology

By

Saba Iqbal

This work reports the oxidative desulfurization of dibenzothiophene in model fuel using Kraft Lignin doped S-graphitic carbon nitride (Fe@KL/S-g-C_3N_4), a newly synthesized and eco-friendly catalyst. Thus, the formation of the composite was confirmed using other characterization techniques such as Energy-Dispersive X-ray Spectroscopy (EDX), Raman Spectroscopy, UV-Visible Spectroscopy, X-ray Diffraction (XRD), Fourier Transform Infrared Spectroscopy (FTIR) and Scanning Electron Microscopy (SEM). The result further showed that Kraft lignin (KL) was well adsorbed on to the S-g-C_3N_4 surface. New functional groups created through Kraft lignin adsorption increase surface coverage, add new active sites and improve S-g-C_3N_4 dispersion. The combined action inside the Fe@KL/S-g-C_3N_4 composite enhances its reactivity and also broadens the optical adsorption range. Optimizing the catalyst's effectiveness and assessing the impact of crucial variables on dibenzothiophene conversion. The following parameters were found to be ideal for maximal sulfur removal (98.37% conversion from 200 ppm): 42.5 °C, 0.3 g of catalyst, 32.5 minutes of reaction time, and 1 ml of H_2O_2 as the oxidant. The quadratic model was shown to be very accurate (R^2 = 0.9905), with a negligible lack of fit (p-value = 0.6671) when compared to the pure error, according to statistical analysis using ANOVA. The heterogeneous catalyst showed exceptional longevity by retaining both its structural integrity and its catalytic properties across five consecutive reuse cycles, proving to be a sustainable choice for desulfurization operations.

Table of Contents

List of Figures

List of Tables

List of Abbreviations

S-g-C_3N_4	Sulfur doped graphitic carbon nitride
KL	Kraft Lignin
Fe@KL/S-g-C_3N_4	Modified Kraft Lignin doped sulfur graphitic carbon nitride
H_2O_2	Hydrogen Peroxide
HDS	Hydrogen desulphurization
ODS	Oxidative desulphurization
PODS	Photo-oxidative Desulfurization
RMS	Response surface methodology
BBD	Box-Behnken design
FT-IR	Fourier transform infrared spectroscopy
UV	Ultraviolet/Visible spectroscopy
XRD	X-ray diffraction
df	Degree of freedom
Std. Dev.	Standard Deviation
DBT	Dibenzothiophene

ECODS	Extractive Oxidative Desulphurization
2FI	2-factor interactions
Cor Total	amount of variation around the mean of the observations
ANOVA	Analysis of Variance

Chapter 1
Introduction

1.1 Background and Significance of Fuel Desulfurization

The petrochemical industry has continued to be the pillar of the world energy sector, meeting more than 80 percent of primary energy demands of the world by use of fossil fuels, which include petroleum-based products [1]. As the world fuel consumption is set to increase by about 1.6 percent a year till 2030, especially in the developing economies, petroleum remains a major source of energy in transport, power generation and industrial consumption. This pressure exerted by this growing demand puts serious strain on the refineries to deliver cleaner and more efficient fuels [2].

A major issue of the contemporary fuel industry is the content of sulfur compounds within crude oil which may take up to 0.05 in sweet crude and above 10 percent in sour oil. When they burn up, they release sulfur oxides (SO_2) which are a major cause of acid rain, particle pollution (PM2.5), and respiratory illnesses [3]. The petrochemical industry contributes a significant portion of the anthropogenic emissions of sulfur dioxide in the world, which leads to the deterioration of the environment and health [4, 5]. In a move to address these issues, regulatory authorities have introduced very low sulfur content in the fuel (10 ppm), like Euro 6 and IMO 2020, and made refineries implement efficient desulfurization approaches to stay in line. Therefore, desulfurization of fuels has become a mandatory activity, not only to comply with the requirements of clean fuels in the world, but also to maintain the competitiveness of industries and their environmental responsibility.

1.2 Environmental and Industrial Impacts of Sulfur Compounds in Fuels

Environmental Impacts:

Sulfur emissions have massive effects on the environment. The SO_2 is released in the air by sulfuric emissions and oxidized in the atmosphere to form sulfuric acid aerosols that lead to the formation of acid rain, lowering the pH levels of soil and water, vegetation damage, and corrosion of infrastructure. In addition, SO_2 also enhances the secondary particulate matter (PM2.5) that is directly associated with respiratory diseases and untimely

deaths [6]. This was demonstrated by the 2020 International Maritime Organization (IMO) sulfur cap that reduced the marine fuel sulfur content to 0.5 percent, reducing the world SO2 emissions by shipping by nearly 80 percent which demonstrated that sulfur regulation was environmentally beneficial [3].

Industrial Impacts:

Sulfur-based compounds also prove to be a significant source of operation at refineries:

- **Catalyst poisoning:** Sulfur deactivates reforming, hydrocracking and other downstream processes which make them more costly to operate [7].
- **Equipment corrosion:** The equipment such as pipelines and reactors is corroded as a result of the H_2S that is formed throughout the processing and increases maintenance expenses.
- **Reduction in the quality of the products:** The products that contain fuels with high levels of sulfur fail to meet the requirements of international standards and their tendency to be sold and exported is low.

Hence, it is not only required to regulate the content of sulfur in fuels to meet the requirements but also to achieve the efficiency of refineries, reduce the risks of the operation, and ensure the competitiveness of the fuel markets in the world.

1.3 Conventional Hydrodesulfurization (HDS) and Its Limitations

Hydrodesulfurization (HDS) has been the workhorse of refinery desulfurization, but in the present energy environment where ultra-low levels of sulfur fuels (10 ppm) are becoming mandatory, it has major constraints. The inability to effectively eliminate refractory sulfur species including 4,6-dimethyldibenzothiophene (4,6-DMDBT) is among its leading challenges. These compounds have a steric hindrance since they are alkyl substituted around the sulfur atom and this hinders their accessibility to the active sites of the traditional HDS catalysts [8, 9]. Consequently, they do not convert fast enough even in high-temperature and high-pressure conditions to meet the current fuel standards.

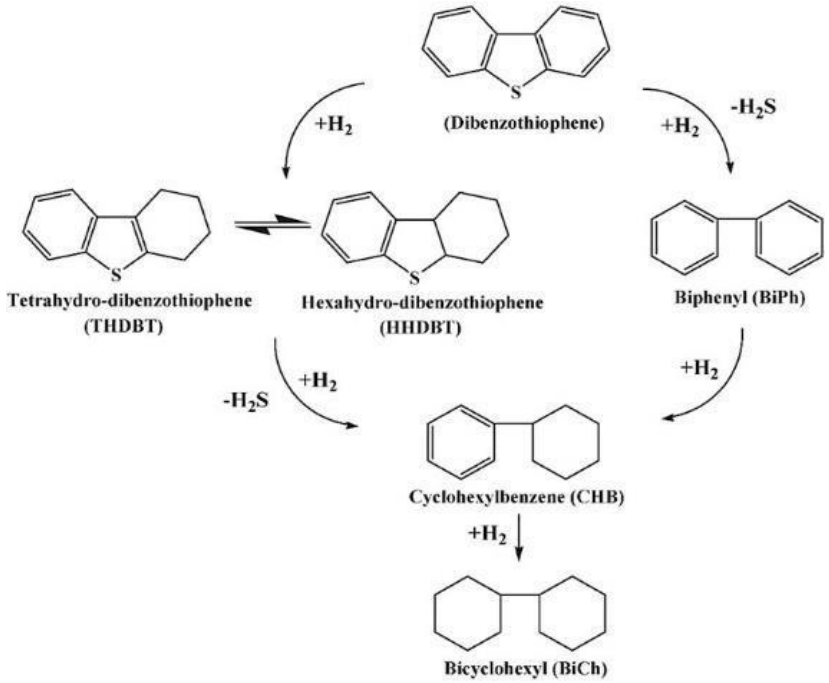

Figure 1. Hydrodesulfurization (HDS) pathways of Dibenzothiophene (DBT).

The other shortcoming is that deep HDS has a huge hydrogen demand. The very process of producing hydrogen itself is energy-demanding and heavily relies on the so-called methane reforming using steam (SMR), which is accompanied by high CO_2 emissions and, thus, negates the environmental advantage of desulfurization. The use of hydrogen also makes operations more expensive, and this is especially applicable in areas where there is a lack of hydrogen infrastructure or natural gas is volatile [10].

Moreover, excessive hydrogenation of fuel components when it is subjected to harsh HDS has unwanted effects on the quality of fuel. Hydrogenating olefins and aromatics, though a stabilizer, decreases the octane ratings in gasoline or cetane numbers in diesel, which may impair engine performance and combustion efficiency. This trade-off is quality that requires a few more refining measures like reforming to replenish octane levels making this process more complicated and expensive [11].

Also, deep HDS units have high capital costs. To achieve ultra-low levels of sulfur, refineries have to install new high-pressure reactors, new catalyst systems, and new facilities to produce hydrogen, and typically require hundreds of millions to billions of dollars of investment per refinery. Such investments are not easily justified in smaller or older refineries particularly in the developing world, hence the inability to generate fuels that meet Euro 6 or IMO 2020 requirements, and this limits their potential market access

[12].

All these undermine the need and urgency to develop renewed and complementary desulfurization technologies that can be more selective of refractory sulfur species, be run at more moderate conditions, and utilize less hydrogen and consume less capital.

1.4 Need for Alternative Desulfurization Methods

Due to the increasing global fuel sulfur limitations and the nature of the conventional hydrodesulfurization (HDS), there is an urgent need to find alternative desulfurization methods that are not only energy saving but also beneficial to the environment. Although HDS is useful in bringing the levels down to acceptable levels, in accordance with previous standards, it proves challenging to achieve the ultra-low levels of sulfur fuel (upto10 ppm) that are required by the recent policies, including Euro 6, or the 2020 sulfur limits provided by the International Maritime Organization (IMO). Its great hydrogen need, harsh working environments and its low capacity to easily eliminate refractory sulfur substances such as 4,6-dimethyldibenzothiophene (4,6-DMDBT) have rendered it increasingly costly and unsustainable. Conversely, new routes like Adsorptive Desulfurization (ADS), Extractive Desulfurization (EDS) [13], Biodesulfurization (BDS) [14], Oxidative Desulfurization (ODS), Photo-oxidative Desulfurization, can all present alternative routes of deep desulfurization at a less harsh and sustainable set of conditions. These approaches are meant to achieve not only the kinetic and thermodynamic limitations experienced in HDS but also lower the hydrogen addiction, work at close to ambient pressure and moderate temperatures and have a better selectivity toward refractory sulfur. Moreover, the methods can be used in combination with implementing renewable or bio-derived catalysts and solvents, which is in connection with the larger objectives of sustainable refinery processes.

1.4.1 Adsorptive Desulfurization (ADS)

Adsorptive Desulfurization (ADS) is an appealing technique that is premised on selective positive adsorption of sulfur-based substances present in fuel feeds onto solid sorbents. In comparison to HDS, ADS does not need hydrogen and stipulates ambient temperature/pressure conditions, meaning that it is energy-efficient by its nature [14]. During this process, the high-surface-area materials (activated carbons, zeolites,

mesoporous silica, and metal-organic frameworks, or MOFs) are used and selectively react with sulfur-based compounds by one of the factors (p-complexation or acid-base reactions, etc.)[15]. Recently, it has been shown that mechanically impregnated adsorbents, especially those incorporating transition metal, e.g. copper, silver and molybdenum can greatly increase the uptake of sulfur through a high affinity to the unsaturated sulfur atom in compounds like dibenzothiophene (DBT) and its derivatives [16].

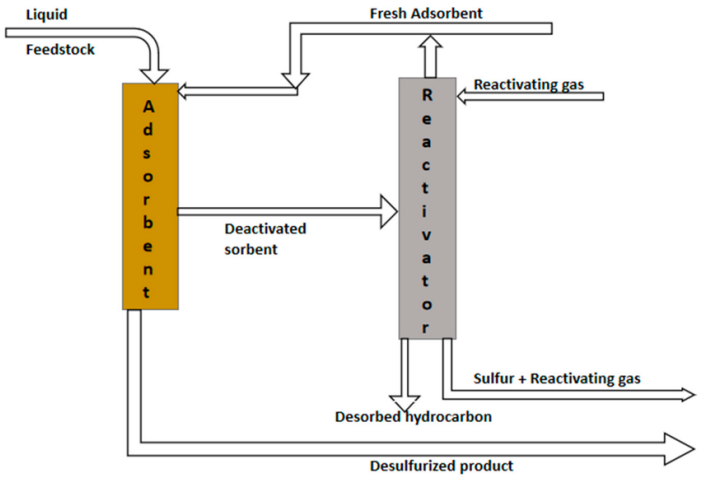

Figure 2. Flow diagram of Bio-desulfurization. [17]

The benefits of ADS are that it is simple and selective in that it can specifically attack refractory sulfur compounds that are not readily removable in HDS. Also, ADS does not distort the hydrocarbon structure of the fuel, which maintains the desirable characteristics of the fuel, including octane or cetane rating [17]. Its industrial use has, however, not been widely adopted as it is said to have problems with adsorbent regeneration, competitive adsorption between aromatic hydrocarbons and reduced efficiency in real-world fuel matrices that consist of complex blends of sulfur species. Other methods like solvent washing and thermal treatment have been tried as regeneration methods but they increase operational complexity and cost [18]. However, further development in the design of adsorbents, in particular the doped nanostructured materials, has demonstrated a significant potential of enhancing sulfur capacity as well as recyclability, with the ADS being a promising secondary step or refining technique to be used after partial HDS treatment as an adjunct.

1.4.2 Extractive Desulfurization (EDS)

Another new method is the Extractive Desulfurization (EDS) which is used to eliminate sulfuric compounds by selective extraction of polar solvents or ionic liquids (ILs) using liquid-liquid extraction [19]. The technique takes advantage of the fact that the solubility of sulfur compounds in polar phase is greater than that of hydrocarbons, effectively isolating them and the fuel on mild conditions. Of special interest have been ionic liquids, which are tunable, have negligible vapor pressure and are chemically stable extraction media [20]. Their capacity to dissolve and store sulfur compounds such as DBT and 4,6-DMDBT with reduced co-extraction of hydrocarbons has been determined in many laboratory studies. Some of the best features of EDS are the ability to operate at almost ambient conditions in terms of temperature and pressure allowing the technology to save a lot of energy and infrastructure expenditure compared to HDS.

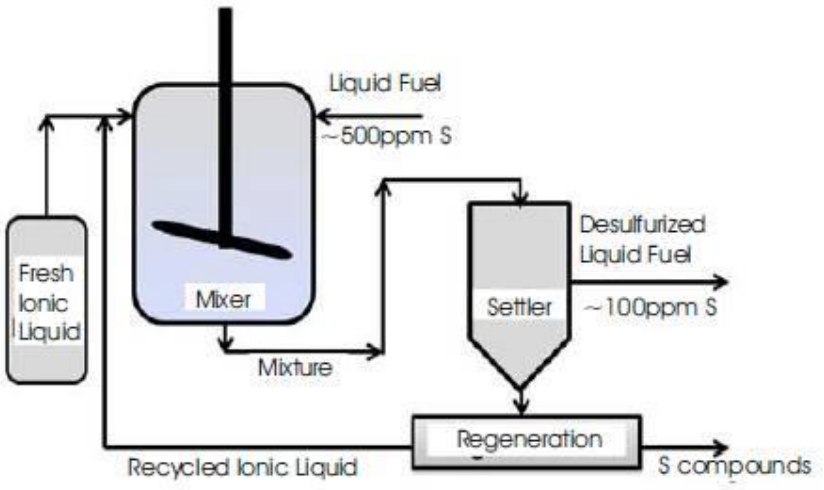

Figure 3. Schematic process of Extractive desulfurization with ionic liquids. [22]

In addition, the technique does not demand the use of hydrogen or catalysts so there is no risk of catalyst deactivation or limitation of hydrogen supply. Nevertheless, commercial use remains under development though, as there are issues with solvent recovery, ionic liquids may be toxic and expensive, and large ratios of solvent to fuel are required in batch processes [21]. Hybrid methods that integrate EDS with oxidation steps or working with task-specific ionic liquids have demonstrated a higher level of sulfur selectivity and lower loss of solvents, indicating that EDS may be an effective desulfurization method in complementary roles in refinery processes.

1.4.3 Bio-desulfurization (BDS)

Bio-desulfurization (BDS) is a biological technology that uses sulfur specific microorganisms or enzymes to selectively remove sulfur atoms of refractory compounds without breaking down the carbon structure of the fuel. The most characterized microbial pathway is the so-called "4S pathway" which is used by microorganisms like *Rhodococcus erythropolis* IGTS8 [22]. The oxidation of dibenzothiophene (DBT) to 2-hydroxybiphenyl (2-HBP) and inorganic sulfite happens via this pathway and maintains the calorific value of the hydrocarbon [22].

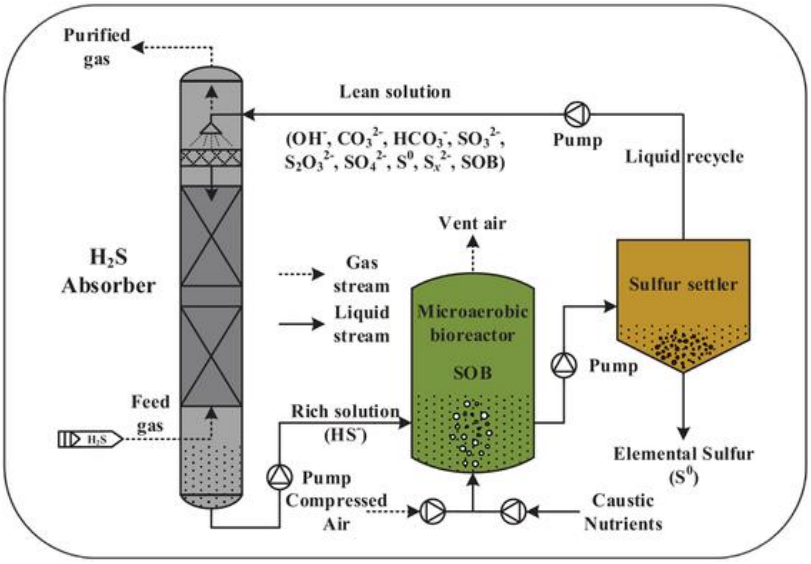

Figure 4. Schematic diagram of biological gas desulfurization. [24]

BDS works in ambient conditions thus making it a good green and low energy choice. Its major advantage is its great specificity: BDS can selectively cleave C-S bonds, but not C-C and C-H bonds in contrast to thermal or chemical methods. This property is especially beneficial in preserving the chemical properties and energy content of fuels [23]. However, BDS has limitations in practice such as low response rates, sensitivity of microbial cultures to organic solvents that are found in fuel, and the end product (2-HBP) inhibition. Research has been done on BDS viability by working on genetic engineering to increase the activity of the enzymes, biocatalysts can be immobilized and reused and two-phase reactor design is done to reduce the impact of toxicity [24]. Despite the fact that not yet commercialized on large scale BDS has potential to be incorporated as a final polishing process in conjunction with partial chemical desulfurization processes, especially to achieve ultra-

deep desulfurization.

1.4.4 Oxidative Desulfurization (ODS)

ODS has also become one of the most promising alternatives to HDS because of its mild condition of reaction and high efficiency with refractory sulfur compounds [25]. It is done by the oxidation of sulfur compounds, e.g. DBT, to their oxides and sulfones using oxidizing agents like hydrogen peroxide or organic peracids and usually a catalyst [25]. These oxidized species are more polar as they are easily extractible or adsorbable. ODS especially works well with alkylated DBT derivatives inaccessible to HDS, with sulfur removal efficiencies of over 90% at conditions that are much harsher than those necessary to process by hydro-processing.

The main focus of the development of ODS is on catalysts. Transition-metal oxides [26], heteropoly acids [27], and supported metal nanoparticles [28] have been investigated as having the property to activate oxidants and select sulfur species. The latest developments involve mesoporous supports and bifunctional catalysts which enhance dispersion and stability thereby improving catalytic turnover and recyclability [26].

ODS does not use hydrogen at all, needs less operational energy, and can be retrofitted into an existing refinery setup as an addition unit compared to HDS. The key obstacles are the price and management of oxidants and the deactivation of catalysts in the repeated cycles.

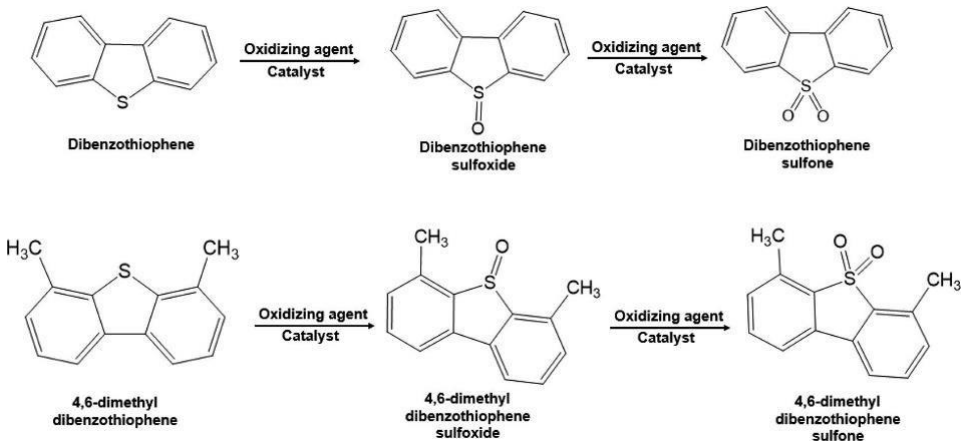

Figure 5. Catalytic oxidation of DBT and related compounds.

However, its suitability in mild conditions and low infrastructure demands make ODS

especially appealing to decentralized refineries and low-cost retrofits to develop the ultra-low sulfur fuel.

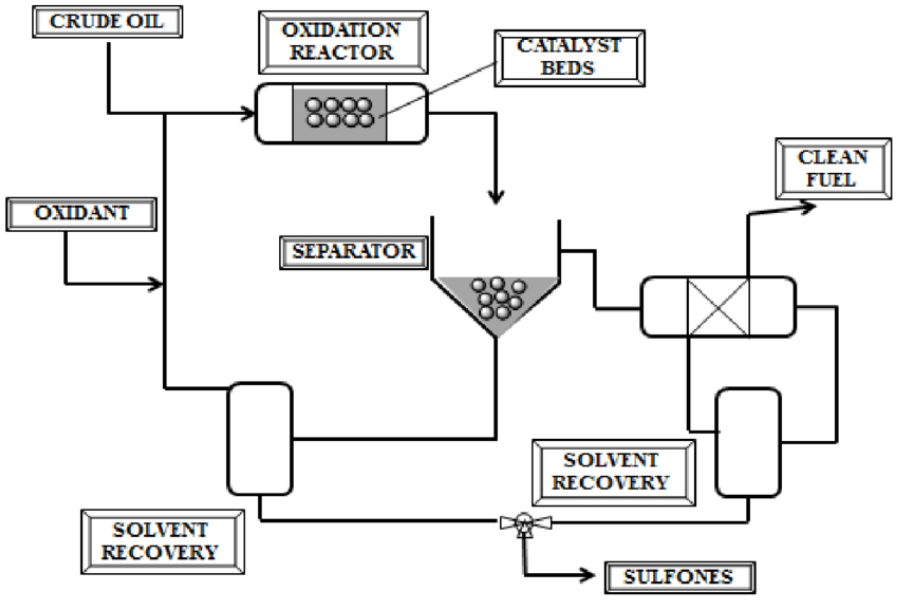

Figure 6. Schematic diagram of Oxidative desulfurization. [31]

1.4.5 Photo-oxidative Desulfurization

Photo-oxidative Desulfurization (Photo-ODS) is a type of photocatalytic desulfurization reaction, which involves the combination of photocatalysis and oxidation to achieve the final sulfur removal through the light as the driving energy. This is a method based on semiconducting photocatalyst (titanium dioxide (TiO_2) and graphitic carbon nitride (g-C_3N_4)) that generate reactive oxidative species under UV or visible light [29]. These reactive species, usually hydroxyl radical, or photogenerated holes, assist the oxidation of sulfur compounds to sulfones or sulfoxides, which are extracted or adsorbed to remove them. The special benefit of Photo-ODS is that it can utilize renewable energy resources including sunlight and, therefore, achieves not only cost effectiveness of energy but also saves greenhouse gas emissions related to thermal treatment. Moreover, it may be used at ambient temperature and pressure, so that it does not require any high-pressure hydrogen systems or higher thermal input. Recent studies have established that heteroatomic (e.g., sulfur, phosphorus) doping of photocatalysts or attaching them to conductive supports can strongly enhance their absorption and catalytic performance in the visible light [30]. As an

example, g-C_3N_4 photocatalysts containing sulfur have demonstrated increased charge separation and high photocatalytic oxidation rates of DBT in the presence of simulated solar light. Nevertheless, Photo-ODS has drawbacks of difficulty in penetration of light in scaled-up reactors, stability of catalysts in repeated cycles, and slower kinetics compared to thermal ODS. These obstacles notwithstanding, their combination with other oxidative or adsorptive procedures has significant future desulfurization systems with low energy requirements, especially in areas where renewable energy is considered a priority in refinery.

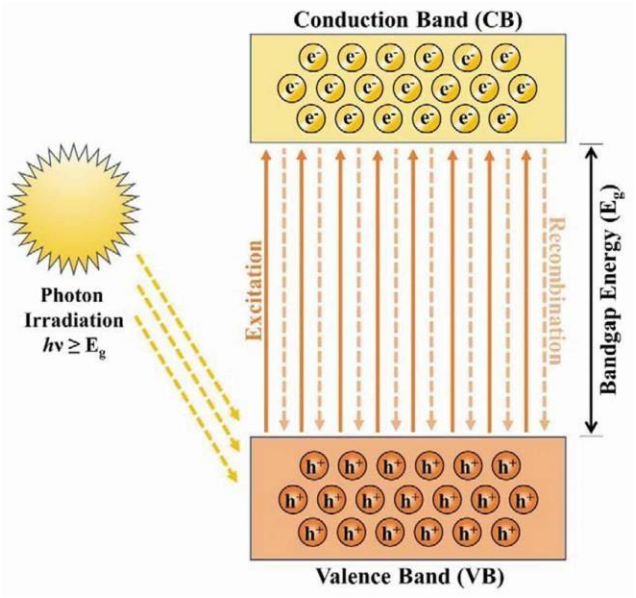

Figure 7. Mechanism of electron-hole pair generation through photonic excitation.

1.5 Oxidative Desulfurization (ODS) as a Sustainable Approach

Oxidative Desulfurization (ODS) has emerged as a leading alternative to conventional hydrodesulfurization for achieving ultra-low sulfur fuels under milder operating conditions and with significantly lower environmental impact. Unlike HDS, ODS does not require high-pressure hydrogen, operating typically at atmospheric pressure and relatively low temperatures (50–80 °C). The process selectively oxidizes refractory sulfur compounds such as dibenzothiophene (DBT) and its alkylated derivatives into more polar sulfoxides or sulfones.

Such oxidized sulfur species may be easily extracted out of the fuel by liquid-liquid extraction or adsorption, and efficacy of over 90 percent may be obtained on sterically

hindered compounds. The ability is especially beneficial to refineries that want to achieve high standards of ultra-low sulfur diesel [31]. Besides, ODS is retrofitted to the existing infrastructure at a small amount of capital compared to HDS units, and thus it is appealing to small to medium-sized refineries, decentralized processes or areas with scarce hydrogen supplies.

1.5.1 Role of Oxidizing Agents (H_2O_2, O_2, etc.)

The selection of oxidants is the core element of ODS and has a significant impact on the reaction kinetics and sustainability of the process. Hydrogen peroxide (H_2O_2) is the best used oxidant because it has a good selectivity, is cheap, and its side effects are water and oxygen, which are harmless. Peracids (peracetic or performic acid) are formed in situ when used together with organic acids like acetic acid or formic acid and serve as powerful oxidizing agents that can take sulfur atoms present in DBT molecules. Studies show that such systems can achieve >90 % desulfurization of model diesel and real high-sulfur diesel under mild conditions (<100 °C, atmospheric pressure), even when subjected to high sulfur loads (>0.8 wt%) [32].

However, the efficiency of H_2O_2 is not simply proportional to its concentration. Excess levels of H_2O_2 may lead to self-decomposition or formation of less reactive radical species (e.g., $HO_2\cdot$), which reduce the overall oxidizing capacity and may inhibit catalyst activity, especially in Fenton-type systems involving iron or manganese ions [33]. Furthermore, oxygen (O_2), organic hydroperoxides like cumene hydroperoxide, and cyclohexanone peroxide have also been explored as oil-soluble alternatives to H_2O_2. While these oxidants offer improved solubility and mass transfer in hydrocarbon media, the in situ formation of peracids remains the most practical due to cost-effectiveness and scalability [32].

Catalyst design plays a synergistic role: supported metal oxides (e.g., α-MnO_2 on palygorskite), tungsten-based materials, or heteropoly acids can activate H_2O_2 more effectively and enhance turnover, enabling high sulfur conversion (>95%) under moderate reaction times and mild conditions. Several recent reports demonstrate that such catalysts retain activity over multiple cycles with minimal deactivation, making ODS both efficient and reusable [34].

Table 1. Comparison table of common oxidants and their oxidation potential

Oxidant	By-product	Active oxygen content (%)
H_2O_2	H_2O	47
HNO_3	NO_X, N_2O, N_2	25.0
$NaClO_2$	NaCl	35.6
t-BuOOH	t-BuOH	17.8
$KHSO_5$	$KHSO_4$	10.5
NaClO	NaCl	21.6
N_2O	N_2	36.4
NaBrO	NaBr	13.4
$C_5H_{11}NO_2$	$C_5H_{11}NO$	13.7
$NaIO_4$	NaI	29.9
PhIO	PhI	7.3

1.5.2 Synergistic Effect of Light Irradiation in Photo-ODS

Photo oxidative Desulfurization is a novel development of traditional ODS in which light irradiation (UV or visible) is added to catalyze oxidative reactions using photocatalysis. Photo ODS: The photocatalysts (e.g. TiO_2 or g-C_3N_4) or doped and unchanged versions of these materials absorb photons to produce reactive oxidative species (e.g. hydroxyl radicals, photogenerated holes) which differentially oxidize sulfur-based compounds to extractable products. Nanoparticle-based photonic activation in combination with chemical oxidants provides the deep desulfurization of ambient pressure and temperature without hydrogen. The strategy helps in using sustainable energy: the activation energy is provided by solar or LED light and this effectively saves on the operating cost and greenhouse gas

emission linked with thermal oxidation. Photocatalysts have been reported to be doped with elements such as sulfur or phosphorus, or attached to conductive supports, to lengthen the light absorption up into the visible spectrum, increase charge separation, and reaction rates. An example is that, when sulfur-doped graphitic carbon nitride is used, it is found to do much better in simulated solar irradiation, attaining deeper oxidation of DBT in fewer time periods and with greater recyclability [31, 35].

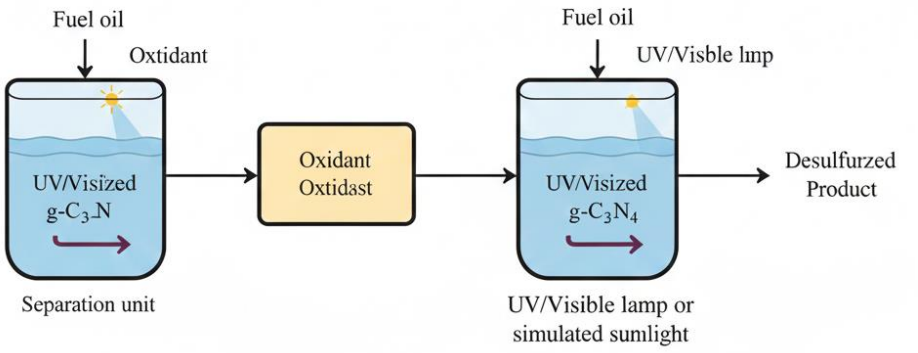

Figure 8. Photo-Oxidative Desulfurization.

Nevertheless, the scale-up issues have not been solved yet: the design of the reactor should provide the efficient light penetration across the fuel matrix, and the catalyst withstand repetitive cycling should be verified [36].

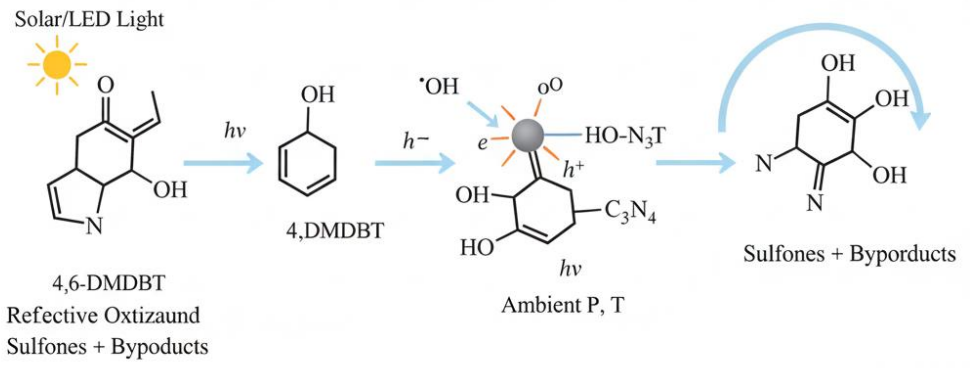

Figure 9. Mechanism of Photo-Oxidative Desulfurization.

These engineering restrictions notwithstanding, Photo ODS remains an exciting technology of sustainable, low-energy desulfurization; in particular, when coupled with oxidative and adsorptive steps, this process can achieve high levels of sulfur removal at

low energy and low environmental costs.

1.6 Graphitic Carbon Nitride (g-C_3N_4): Properties and Potential

Graphitic carbon nitride (g-C_3N_4) has received considerable credit as a free metal semiconductor photocatalyst because of its low cost, ease of preparation, chemical stability, and activity in the visual light. It is generally produced by thermal polymerization of nitrogen-containing starting materials like melamine, dicyandiamide or cyanamide, and a polymeric layered material formed by tri-s-triazine structures is obtained [37].

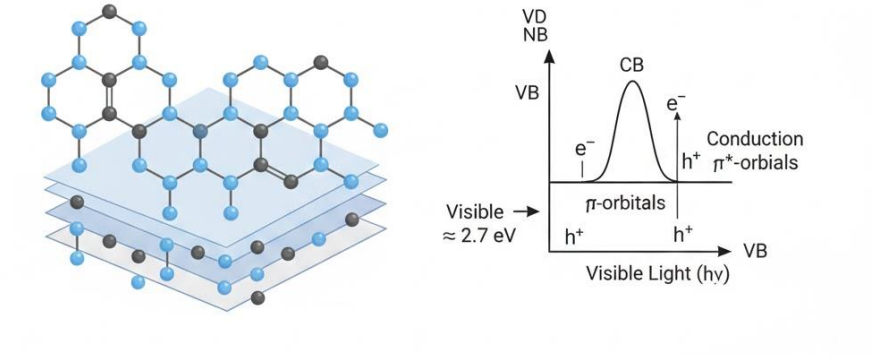

Figure 10. Molecular and electronic structure of g-C_3N_4.

It is a structure in which the C and N atoms are all sp^2-hybridized to form a p-conjugated net giving it a high thermal and chemical stability. Having a band gap of 2.7 eV, g C_3N_4 is able to efficiently absorb visible light and produce electron-hole pairs that are able to cause redox reactions. All these properties predispose it as a good candidate of sustainable photocatalytic reactions, such as hydrogen evolution, CO_2 reduction and oxidative desulfurization of fuels. Its non-metallic composition also makes it compatible to the environment and economically viable when used on mass scale [38].

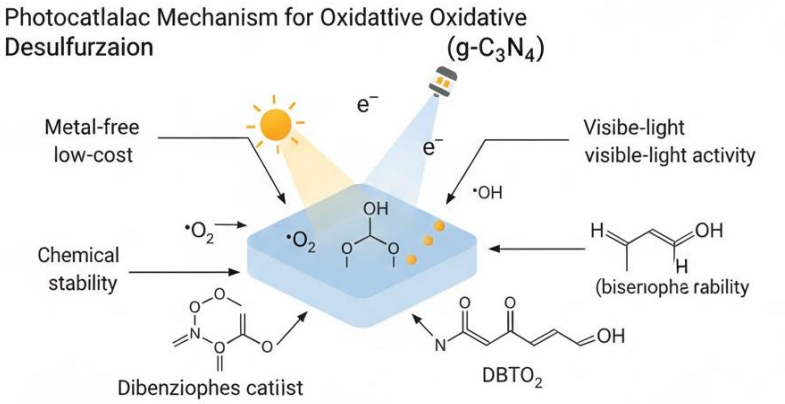

Figure 11. Photocatalytic mechanism for ODS.

1.6.1 Structure and Photocatalytic Mechanism of g-C_3N_4

Graphitic carbon nitride (g-C_3N_4) has received a lot of interest as a semiconductor photocatalyst with no metals because of its low cost, easy synthesis, chemical stability and visible light activity. It is commonly prepared by thermal polymerization of compounds rich in N, to produce a polymeric layered substance based on tri-s-triazine units. This building consists of a p-conjugated network of sp^2-hybridized carbon and nitrogen atoms, and it gives the building remarkable thermal and chemical stability.

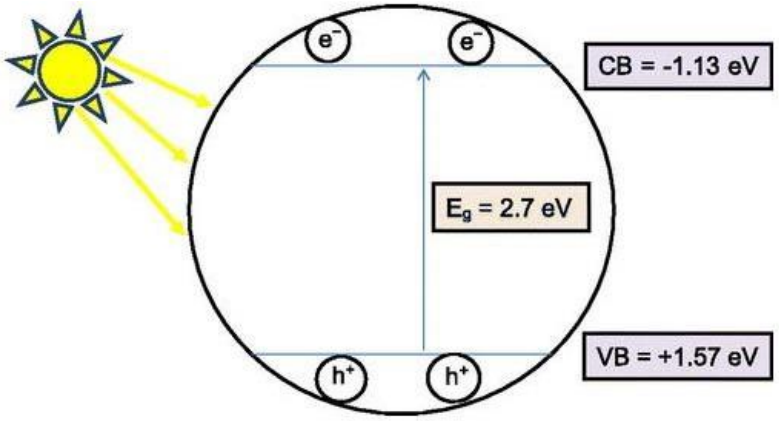

Figure 12. A typical charge transfer mechanism for g-C_3N_4.

Having a band gap value of about 2.7 eV, g-C_3N_4 is able to absorb the visible light efficiently and produce electron-hole pairs that can initiate redox reactions [39]. These characteristics render it an attractive candidate in sustainable photocatalytic reactions, such as hydrogen evolution, CO_2 reduction, and oxidative desulfurization of fuels.

The fact that it is made of metal-free material also improves its compatibility with the environment as well as its economic competitiveness in large-scale applications. g-C_3N_4 is made up of heptazine (tri-s-triazine) units with planar amino links, which create a two-dimensional material in layers and has a conjugated system of electrons.

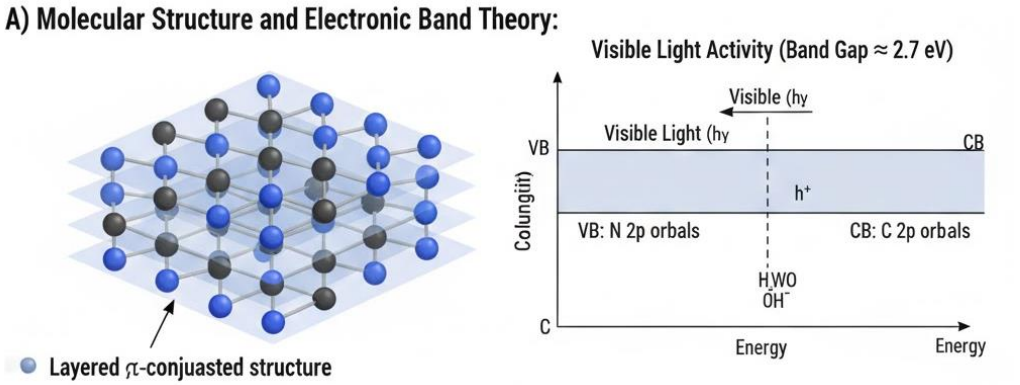

Figure 13. Molecular structure and band theory.

An electron-hole pair is formed when the electrons on the valence band (The nitrogen 2p orbitals predominate in the valence band) are excited to the electrons on the conduction band (The carbon 2p orbitals predominate in the conduction band) through the irradiation of the electrons by visible light [39]. Photogenerated carriers can undergo surface redox processes: Reduction of the adsorbed species, e.g. oxygen, to superoxide radicals by electrons, and oxidation of holes by an electron donor or target molecule [40]. Nitrogen vacancies or surface defects in g-C_3N_4 are known to serve as center of charge trapping, enhancing the separation of charge and increasing carrier lifetime, which increases g-C_3N_4 photocatalytic activity [41]. It also has an amine surface that would promote adsorption and activation of reactant molecules and would enhance its catalytic effect. The oxidative desulfurization process of g-C_3N_4 is of interest to the photocatalytic mechanism because photoexcited electrons and holes create reactive oxygen species that can oxidize sulfur compounds like dibenzothiophene into more polar sulfones and sulfoxides. It is then possible to recover these products easily off the hydrocarbon matrix, allowing efficient deep desulfurization at mild conditions.

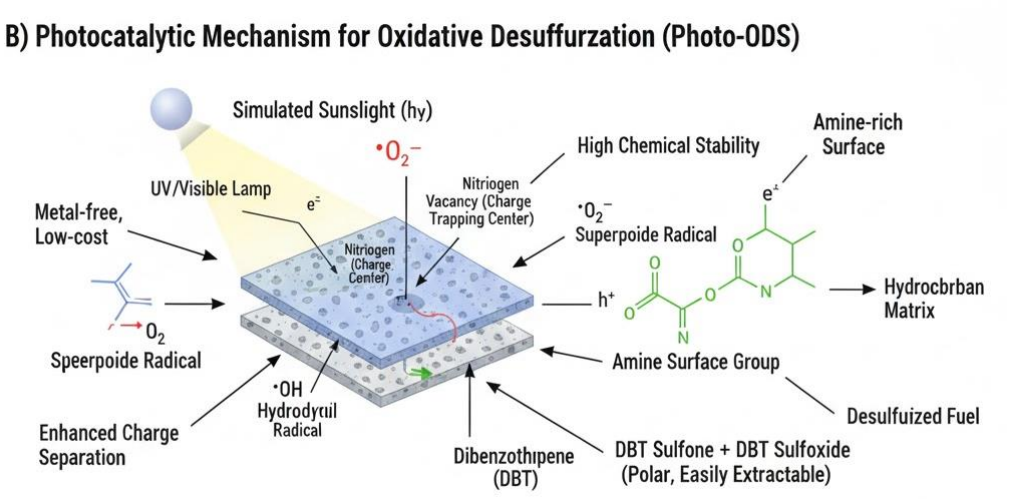

Figure 14. Photocatalytic mechanism for ODS.

1.6.2 Limitations of Pristine g-C_3N_4

Although it has benefits, pure g-C_3N_4 has several internal shortcomings that limit its photocatalytic activity. It contains a relatively low surface area that is normally less than 10 m2/g and hence restricts the number of active sites of the reactions [42]. In addition, the quantum efficiency of photogenerated electron-hole pairs is greatly lowered by the rapid recombination of particles [43]. Its optical absorption is within the spectral range of shorter wavelengths (below 460nm), and a large part of the solar spectrum is not used [40]. It is also limited in catalytic versatility as its oxidation strength is moderate and is thus limited to producing highly reactive radicals. This has also been a disadvantage as it is very low in terms of charge mobility considering the low crystallinity and grain boundary effects, which slow down the rate of effective charge transfer in the material [44]. Catalyst recovery may also prove difficult in the liquid-phase reactions due to its fine particle size and by way of aggregating [45]. Such restrictions require transformation measures including elemental doping, heterojunction development, defect engineering and nano structuring to enhance its light absorption spectrum, charge partitioning efficiency, as well as catalytic activity in general. With these limitations being addressed by making specific adjustments, g-C_3N_4 can be turned into an efficient photocatalyst, especially in a process of photo-oxidative desulfurization where catalysis by visible light at ambient temperature represents a feasible and sustainable and efficient route to producing ultra-low-sulfur fuels.

1.7 Modification Strategies to Enhance g-C_3N_4 Efficiency

Even though pure graphitic carbon nitride (g-C_3N_4) bears good photocatalytic performance, its potential is hampered by the factors, which include fast electron-hole recombination, low specific surface area, and limited capability in absorbing visible light. In order to eliminate these constraints, a number of modification plans have been established to advance its photocatalytic capability and expand its usefulness in environmental and energy related procedures such as oxidative desulfurization. Elemental doping, coupling with carbonaceous materials and introduction of structural defects are among the most effective methods [46]. These are strategies that are aimed at fine-tuning the electronic structure, enhance light harvesting functions, facilitate charge carrier separation, and enhance active catalytic sites.

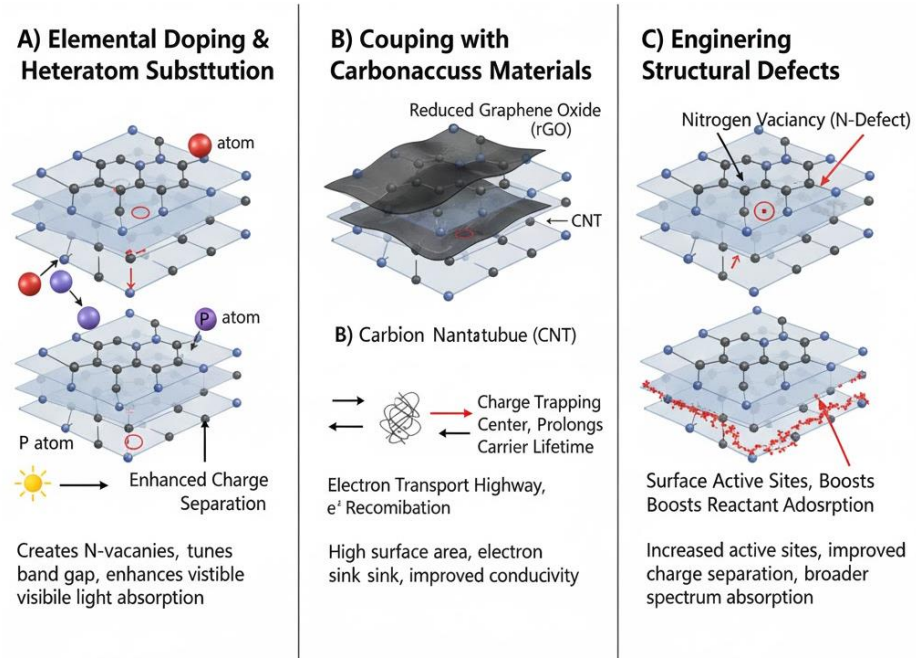

Figure 15. Modification strategies for improving efficiency of g-C_3N_4.

1.7.1 Elemental Doping (S, P, etc.)

Another method, which is widely used to alter the electronic and optical characteristics of g-C_3N_4, is elemental doping. The heteroatomic doping (e.g., with sulfur (S), phosphorus (P), boron (B) or oxygen (O)) contains foreign atoms in g-C_3N_4 lattice, changing the band structure and extending the range of light absorption to visible [47]. As an example, the

doping of sulfur substitutes part of the nitrogen sites to form mid-gap states, which reduces the band gap and enhance the use of visible light [48]. Instead, phosphorus doping is an addition of electron donor sites that increase charge density and generate easy electron transfer, an essential reaction in photocatalytic reactions including oxidative desulfurization [49]. Also, dopants may serve as active centers, which mediate the adsorption and activation of reactant molecules. As an illustration, g-C_3N_4 has been sulfur-doped and its oxidation abilities of dibenzothiophene have been enhanced because of a higher level of interaction between the catalyst surface and the sulfur-containing compounds. In addition, doping may decrease charge recombination by forming localized energy states that confine charge carriers and prolong their lifetime and increase redox activity [50]. On the whole, elemental doping is a relatively easy and yet efficient way of enhancing the light absorption and catalytic activity of mild conditions.

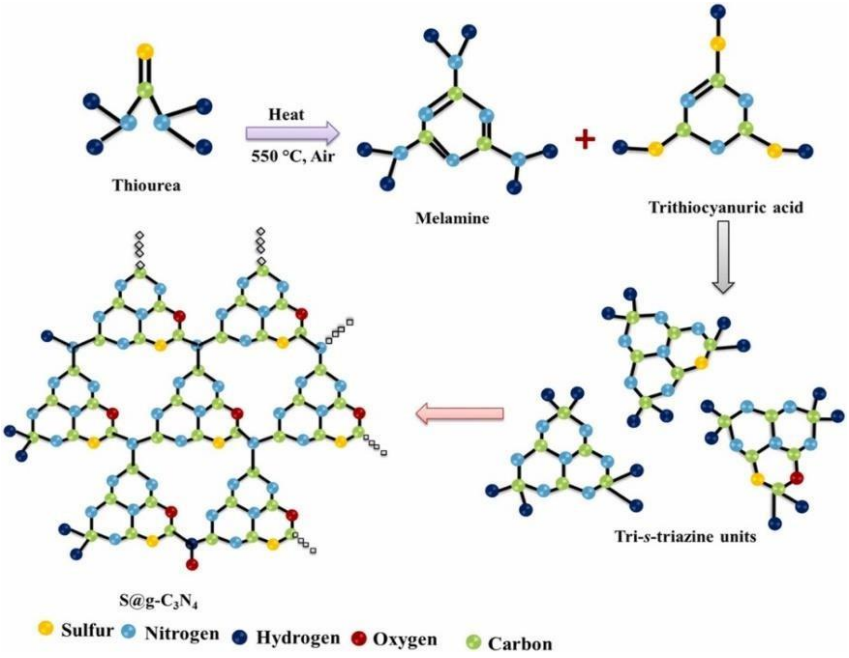

Figure 16. Schematic representation of the synthetic procedure of S@g-C3N4.

1.7.2 Coupling with Carbonaceous Materials

g-C_3N_4 when coupled with carbon-based substances like graphene, carbon nanotubes (CNTs), activated carbon or bio-based carbon structures is much more conductive and better in separating charges [29]. Carbonaceous materials have great surface areas and high

electron mobility and thus they can be used as conductive support or electron sinks that minimize recombination of photogenerated electron-holes pairs. These materials are used to make heterostructures or intimate interfaces with g-C_3N_4, which support the rapid transport of photoexcited electrons in the g-C_3N_4 to the carbon phase to improve photocatalytic activity [51]. Graphene-g-C_3N_4, such as, have been shown to have a better oxidative desulfurization efficiency with its synergistic characteristics: the graphene sheets provide conductive network and high adsorption sites, whereas g-C_3N_4 offers photoactivity in the visible light. By analogy, its coupling with lignin-based carbon or biochar also creates vast numbers of functional groups (e.g., hydroxyl and carboxyl) which further enhance DBT adsorption and oxidation [52]. Not only are these carbonaceous hybrids more active catalysts, but they also enhance structural stability and recyclability, which makes them especially appealing to take part in the purification of sustainable fuels.

1.7.3 Introduction of Structural Defects

The other effective method of g-C_3N_4 activity improvement is defect engineering. The structural defects may also act as trap sites, including nitrogen vacancies or carbon vacancies, that increase the lifetime of the photogenerated carriers and act as an extra site, where catalytic reactions take place. Such defects may be created by thermal processes, chemical etching, or the non-stoichiometric synthesis. The vacancy of nitrogen (especially) produces the localized states at the conduction band edge that enhance the process of electron transport and visible-light absorption [53]. In addition, the defect sites usually have unsaturated coordination environments that make them highly chemically reactive and able to absorb reactant molecules. As an illustration, the g-C_3N_4 containing a high number of defects has exhibited faster oxidation rates of refractory sulfur compounds as a result of the increased rate of charge transfer and enhanced accessibility to target molecules [54]. Nevertheless, the generation of defects in large amounts can undermine the structural integrity and stability so that a reasonable balance between reactivity and durability must be reached by the controlled generation of defects [54].

These strategies of modification, namely: elemental doping, carbonaceous coupling and defect engineering are usually used in a synergistic fashion to attain better catalytic performance. An example is the use of sulfur-doped g-C_3N_4 with bio-derived carbon

because it has a longer light absorption and increased charge separation [55], in addition to having plenty of adsorption sites of sulfur compounds, and is therefore very efficient in photo-oxidative desulfurization. These combined strategies are in line with the sustainable energy targets and provide directions of efficient, low cost and environmentally friendly desulfurization processes.

1.8 Sulfur-Doped g-C_3N_4 (S-g-C_3N_4): Photocatalytic Advantage

Graphitic carbon nitride (g-C_3N_4) that is sulfur-doped (S-g-C_3N_4) has proved to be a very useful modification of pure g-C_3N_4 [48], especially in oxidative processes in photocatalysis like its use in oxidative desulfurization. Sulfur doping causes great alterations in the electronic structure, surface chemistry and optical property of g-C_3N_4. Light absorption in the visible band is further extended as the sulfur atoms replace the nitrogen or carbon positions in the lattice, forming localized states in the band gap, and bringing the energy of the band gap closer to the visible region [56]. This enhanced light collection is imperative in effective use of solar spectrum in ambient conditions. Besides the modification of the band structure, sulfur atoms create sites of higher electron density that render them interacting more with the target molecules , especially organosulfur molecules such as dibenzothiophene (DBT) and its derivatives [57]. The heteroatom doping interferes with the natural symmetry of the g-C_3N_4 that creates defect sites and high surface-active centers and promotes adsorption and subsequent catalytic reactions. Moreover, the doped sulfur will be able to change the charge carrier dynamics by decreasing the electron-hole recombination rates by creating shallow traps that increase carrier lifetimes [57]. All of these effects greatly enhance the photocatalytic efficiency of g-C_3N_4 in the sense that S-g-C_3N_4 is an even better candidate in the event of sustainable desulfurization.

1.8.1 Mechanistic Insights of S-g-C_3N_4 in Oxidation Reactions

The oxidation reaction of S-g-C_3N_4 by photocatalytic action comprises synergies due to its modified electronic structure of enhanced surface chemistry. When irradiated in visible light, S-g-C_3N_4 has a higher photon absorption capacity than pristine g-C_3N_4[48], since the band gap is narrower, and electrons are excited by the photon to the conduction band (CB)

and holes generated in the valence band (VB), thereby. The dopants are sulfur and produce mid-gap states which are either electron donors or acceptors that allow faster charge transfer and recombination losses are minimized. These electrons and holes produced by photogenic processes are involved in redox reactions that are important in oxidative desulfurization [58]. The electrons react with dissolved oxygen molecules to produce superoxide radicals (O2-), the holes react with water or hydroxide ions to produce hydroxyl radicals (OH) or directly react with sulfur-containing compounds. These reactive oxygen species (ROS) along with holes formed by photogeneration assault the sulfur atom of DBT and analogs, transforming it into polar sulfoxides and sulfones. The products of these oxidations are more polar and can be readily removed out of the hydrocarbon phase, producing deep desulfurization with neither the use of hydrogen nor high temperatures. Furthermore, sulfur incorporation of the g-C_3N_4 structure promotes the adsorption of organosulfur species due to positive sulfur-sulfur or sulfur-p interactions, which essentially concentrates the reactants on the catalyst surface and increases the reaction rate. Sites created during doping also encourage activation of oxidizing agents, e.g. hydrogen peroxide, thereby enhancing the oxidation reaction. Recent reports have described that S-g-C_3N_4 can desulfurize DBT with a high efficiency of over 90% with the use of visible-light and mild reaction conditions and this indicates its practical use as a refinery agent towards the production of ultra-low-sulfur fuels [59]. All in all, enhanced light absorption, separation of charges, and active sites of S-g-C_3N_4 all lead to the high efficiency of photocatalytic activity of the material in comparison to g-C_3N_4. These features render it a central substance towards the design of clean and green desulfurization processes.

1.9 Lignin as a Renewable Catalyst Support

Lignin, an abundant biopolymer derived from plant cell walls, has recently gained attention as a sustainable and renewable material for catalytic applications. As one of the three main components of lignocellulosic biomass (alongside cellulose and hemicellulose), lignin accounts for approximately 15–30% of the dry weight of biomass and represents the largest natural source of aromatic carbon on Earth [60]. Despite its high availability, lignin has historically been treated as a low-value byproduct of the paper and pulp industry [61], where it is primarily combusted for energy recovery.

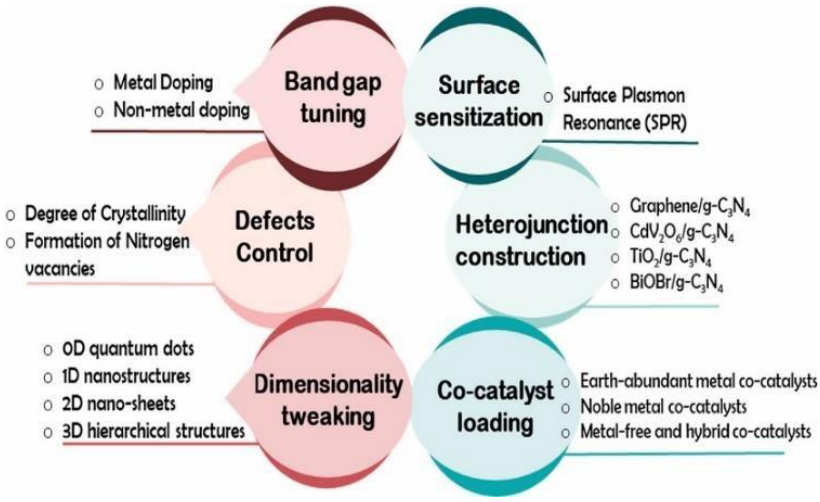

Figure 17. Illustration of different strategies for improving catalyst performance.

However, recent advances in green chemistry and biomass valorization have shifted focus toward its potential as a precursor for functional materials [62], including its role as a support in heterogeneous catalysis.

Lignin is particularly attractive as a catalyst support due to its renewable nature, low cost, chemical versatility, and rich content of functional groups such as hydroxyl, methoxy, and phenolic groups [63]. These functionalities allow lignin to interact strongly with catalytic species and facilitate their immobilization or dispersion on its surface. Moreover, lignin-derived supports exhibit a unique porous carbonaceous structure after thermal or chemical activation, providing a high surface area and abundant active sites favorable for catalytic processes [63]. As a biomass-derived material, lignin also contributes to the development of environmentally friendly catalytic systems by reducing dependence on non-renewable and expensive inorganic supports such as silica or alumina [64].

1.9.1 Structure and Properties of Kraft Lignin

The most common technical lignin is the kraft lignin which is a byproduct of kraft pulping process. It is very heterogenous in structure and is mainly composed of three phenylpropanic monomers namely p-coumaryl alcohol, coniferyl alcohol and sinapyl alcohol. These monomers are p-hydroxyphenyl (H), guaiacyl (G), and syringyl (S) units, respectively, and are interconnected with the help of different ether (b-O-4) and carbon-carbon bonds. The pulping of the kraft further adds more sulfur-based functionalities to the

lignin framework and further alters its chemical reactivity [65-68]. The complexity of the aromatic rings, hydroxyl groups and the aliphatic chains in kraft lignin form a complex three-dimensional network [69]. The structure of this type of carbon nanoparticles gives it a number of desirable characteristics, including thermal stability, high carbon content, and the presence of reactive functional groups that can be further modified or functionalized. Notably, its hydroxyl groups are phenolic and aid in a redox reaction and transmission of electrons, which are beneficial in catalytic activity [70]. It is also an outstanding precursor to the produce of activated carbon material with high surface area and tunable porosity due to its inherent aromatic nature and can be used as a strong support of metal nanoparticles or photocatalytic material in essence.

1.9.2 Lignin-based Supports in Catalysis

The lignin and its derivatives have demonstrated considerable potential as support in heterogeneous catalysis because of the high-density of functional groups [13] and adjustable surface chemistry [71]. Lignin when carbonized or modified by chemicals, makes porous carbonaceous supports that can hold the active metal species including Fe, Co, Ni, or even noble metals such as Pd and Pt [72]. These support materials are produced by lignin, which improves the dispersion of the metal particles and inhibits aggregation to increase catalytic performance. In addition, natural oxygen- and sulfur-containing groups present in lignin can be utilized as anchoring groups to the catalytic species to enhance the contact between the support and the active phase. Carbonaceous support (lignin-derived carbonaceous support) has been effectively combined with semiconductors including graphitic carbon nitride (g-C_3N_4) in photocatalysis [73].

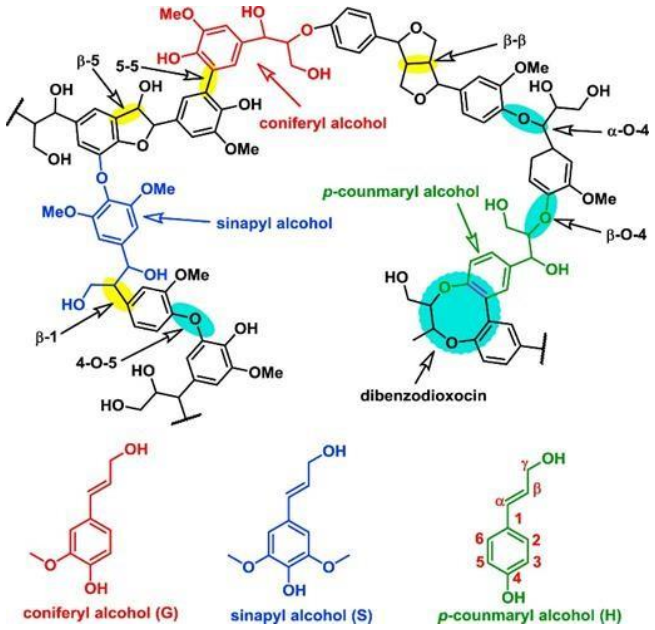

Figure 18. Representative structures of lignin and its constituent monolignol units.

The resulting composites advantageously have enhanced electron transfer pathways, an extended light path, and the lignin matrix has added active sites. As an example, g-C_3N_4 catalysts supported on lignin have been shown to exhibit an increased activity during oxidative desulfurization in which the surface characteristics of lignin enhance the adsorption of organosulfur species and at the same time enhance the dynamics of charge separation of the photocatalyst. Besides, the renewability and biodegradability of lignin are also sustainable and can be used to provide an alternative to the conventional synthetic supports which are environmentally hostile. In general, not only is the lignin integration as a catalyst support beneficial because it allows the valorization of a low-cost industrial byproduct, but it also helps develop green and economical catalytic systems. Its structural peculiarities, its abundance, and extractability make lignin a potential source of material in the next generation of catalytic uses in the purification of fuels and in environmental cleansing.

1.9.3 Extraction Methods

Several procedures are used to separate lignin out of the lignocellulosic biomass and each of them results in lignin that is characterized with different structural and chemical properties:

- **Kraft Pulping:** It is a popular technique in industries whereby wood chips are digested using sodium hydroxide and sodium sulfide in high temperatures. It produces kraft lignin, sulfur containing yet condensed kraft lignin, but very available [74].
- **Organosolv Extraction:** Organizational solvents (ethanol, methanol, acetone) are utilized in either acidic or neutral environments, typically containing catalysts (e.g. sulfuric acid). It yields sulfur-free low molecular weight lignin that can be utilized in high value [75].
- **Soda Pulping:** It uses sodium hydroxide alone and the process is normally used in herbaceous or non-woody biomass. It gives high phenolic sulfur-free lignin [76].
- **Acid Hydrolysis:** The biomass remains with the dilute acids that hydrolyze the hemicellulose and cellulose to leave behind the lignin. This technique is primarily applied in bioethanol production residues in biorefinery [76].
- **Enzymatic Hydrolysis Residues:** In biochemical biorefineries, cellulose and hemicellulose are hydrolyzed by enzymes to sugars, and the lignin is hydrolyzed to leave a residue that is insoluble, and which contains more functional groups and reduced structural condensation [77].

1.10 Integration of Lignin with S-g-C_3N_4 for Sustainable Catalysis

The addition of lignin on sulfur-doped graphitic carbon nitride (S-g-C_3N_4) is a new strategy of creating economical, renewable, and efficient photocatalysts towards the purification of fuels in sustainable processes. Such a combination takes advantage of the complementary characteristics of the two materials the high level of photocatalytic performance of S-g-C_3N_4 and the renewable, functionalized carbon-rich lignin structure [78]. Lignin also acts as a strong support or co-catalyst by boosting the stability, surface area and electron transfer features of S-g-C_3N_4. This is because of the porous and functionalized structure that contains a high number of hydroxyl, methoxy, and phenolic groups that promote the strong interaction of S-g-C_3N_4 nanosheets or particles and result in their uniform dispersion. These reactions inhibit the agglomeration of S-g-C_3N_4, which results in more active sites available to the reaction in photocatalysis. Also, the aromatic web of lignin, after being carbonized,

provides a conductive skeleton that promotes an efficient separation of charge by being an electron mediator which lowers the rate of recombination among photogenerated carriers. Sustainability wise, using lignin will be valorizing a low cost, high-volume industrial byproduct, which is in line with the concept of green chemistry. Recent reports have established that lignin-based S-g-C_3N_4 composites have a better yield in oxidative desulfurization of refractory sulfur compounds like dibenzothiophene in visible- a light irradiation. The synergistic process can be explained by the fact that lignin can adsorb sulfur compounds stronger and increase the process of charge transfer in S-g-C_3N_4. This combination does not only help overcome the shortcomings of pure photocatalysts but also delivers circular catalysis and utilization of biomass-derived substances into energy and environmental use, rendering it a good avenue towards sustainable catalysis.

1.11 Response Surface Methodology (RSM) for Process Optimization

Response Surface Methodology (RSM) is an effective and robust statistical and mathematical technique applied in modeling, analyzing and optimization processes where any number of input variables are the ones that affect a response or an output. In catalytic research, RSM is widely used in order to identify the best conditions that will maximize the catalytic performance and minimize the number of experiments and use of resources [79].

RSM is performed by exposing experimental parameters to a sequence of variations and a subsequent fit of the observed data to a second order model based on the relationships between the variables and the responses. It has mostly found application in photocatalysis and chemical reaction engineering where interactions between various factors (catalyst dosage, oxidant concentration, reaction time, temperature and light intensity) can be nonlinear and complex [80]. Using RSM, the researchers will be able to test the effect of each of these variables and their interaction, reveal the most important ones, and define the optimum range of these variables that will result in high catalytic efficiency.

Applied in the context of oxidative desulfurization RSM is useful in determining the optimal combination of the operational parameters including catalyst loading, dosage of hydrogen peroxide and irradiation time that allow the best sulfur removal rates. It is a

statistical method that minimizes the experimental costs and maximizes the reproducibility and makes it possible to optimize catalytic processes using the data in real-world constraints.

1.11.1 Overview of RSM in Catalytic Studies

In catalytic research, RSM is primarily employed to optimize reaction conditions by developing an empirical model that correlates the input parameters with the desired performance metrics (e.g., desulfurization efficiency, reaction rate). Three primary steps are used in the methodology: the design of the experimental plan, experimental experiments according to the design matrix, and data fitting to the second-order polynomial regression model. The overall equation of the quadratic regression model is:

$$Y = \beta_o + \beta_i X_i + \beta_{ii} X_i^2 + \beta_{ij} X_i X_j + \varepsilon \qquad \text{Eq. 1}$$

In this equation:

- Y represents the response variable.
- X_i and X_i^2 are the independent input variables.
- β_o is the intercept constant.
- β_i represents the linear coefficients.
- β_{ii} represents the quadratic (squared) coefficients.
- $\beta_{ij} X_i X_j$ represents the interaction coefficients.
- ε is the random error term.

The model enables one to visualize the response in the form of contours and 3D surface graphs which are useful in making meaningful conclusions about the relationship between factors and response. There is a long history of RSM optimization of heterogeneous photocatalytic reactions, such as pollutant degradation [81] and oxidative desulfurization , in which it is effective at pinpointing any synergy between operating variables.

1.11.2 Box-Behnken Design (BBD) Approach

The Box-Behnken Design (BBD) represents one of the most widespread types of RSM designs and is used because of its effectiveness and applicability to quadratic response modeling. In contrast to central composite designs, BBD does not utilize experiments in the extreme corners of the experimental space which is helpful in avoiding undesirable or unsafe experimental conditions. Rather it deals with points that are located at the half-way points of the edges of the experimental domain and at the center, being resource-efficient in this regard [82]. BBD commonly takes three values (low, medium and high) of each variable and is best suited to studies of three or four independent factors at the same time in catalysis. To desulfurize with S-g-C_3N_4 composites, which contains lignin, BBD was used to carefully test the impact of catalyst loading rate, oxidant concentration, duration of irradiation and initial concentration of sulfur on desulfurization. The strengths of BBD are: Less experimental runs than full factorial designs [83]. Large accuracy in the estimation of quadratic terms and interaction.

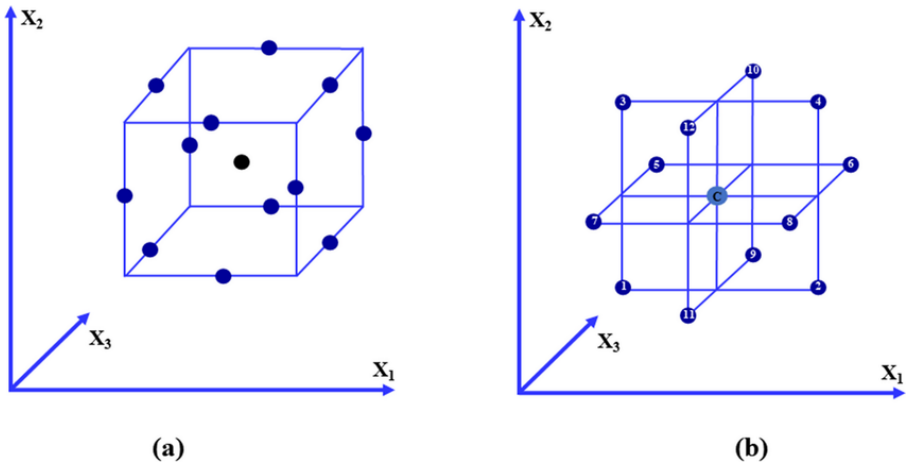

Figure 19. Box Behnken design representation with three factors. [84]

The advantage is that it is safer and more practical since it is not subjected to extreme experimental conditions. Therefore, the best conditions of reaction to be used where maximum amount of sulfur is removed can be determined using less experiments, saving on time and resources used but maintaining accuracy. The method is thus appropriate in perfecting the process of photocatalytic desulfurization and commercializing the process in large scale.

1.12 Objectives of the Study

The main aim of the paper is to design an efficient, sustainable, and environmental-friendly photocatalytic process of deep desulfurization of model fuel oil with the help of a modified lignin-supported sulfur-doped graphitic carbon nitride (Lignin@S-g-C_3N_4) catalyst. The experiment seeks to combine the renewable character of lignin and the new state-of-the-art photocatalytic characteristics of S-g-C_3N_4 to overcome the vulnerability of conventional hydrodesulfurization (HDS) and fulfill highly desired ultra-low sulfur fuel standards. Through a visible-light-powered photo-oxidative desulfurization (Photo-ODS) strategy, the work aims to offer a solution to the energy-efficient alternative to the current desulfurization methods, which is likely to decrease the operational costs and the effects on the environment. The particular aims of this study can be stated in the following way:

1. **Modification and synthesis of catalyst:** To prepare sulfur doped g-C_3N_4 and combine it with kraft lignin as a renewable support material, and consequently, increase photocatalytic activity, stability, and surface area.

2. **Catalyst Characterization:** Catalysts are any substances or species capable of catalyzing a chemical reaction. To carry out structural, morphological, and surface analysis of the prepared Lignin@S-g-C_3N_4 composite with techniques, including FTIR, Raman spectroscopy, XRD, UV-Vis spectroscopy, SEM/EDX, and XPS analysis to learn about its physicochemical properties.

3. **Assessment of photocatalytic performance of desulfurization:** To evaluate the effectiveness of the synthesized catalyst in the oxidative desulfurization of model fuel oil which includes dibenzothiophene (DBT) under the radiation of visible light concentrating on a high percentage of sulfur removal under the mild conditions.

4. **Streamlining of process parameters:** To maximize the important operating variables which include catalyst loading, concentration of oxidant (H_2O_2), reaction time, and light irradiation by using Response Surface Methodology (RSM) and Box-Behnken Design (BBD) to give maximum desulfurization efficacy.

5. **Sustainability assessment: Recyclability:** To determine the stability and

reusability of the catalyst through several rounds of desulfurization as well as determining its viability in terms of industrial scale uses as a sustainable alternative to the traditional approaches.

Through these objectives, the study would help in the development of green catalytic technologies to produce ultra-low sulfur fuels and at the same time would value lignin, which is a large industrial byproduct, to a value-added constituent of high-performance catalytic systems.

Chapter 2
Literature Review

The main aim of the work was to produce a highly doped molybdenum nitride and sulfur-doped graphitic carbon nitrite nanocomposite, denoted as MoN@S-GCN, that can be greatly used as an electrochemical sensor of the chloramphenicol (CAP) which is a broad-spectrum antibiotic. Molybdate nitride is an element which has received a lot of interest in electrocatalytic processes because of its high electrically conductive properties, mechanical stability and corrosive resistance. MoN nanorods were prepared in this paper by using a pyrolysis and ultrasonication technique in a one-step process to incorporate them into the S-GCN nanosheets. The combination of MoN with S-GCN increased the electrochemical characteristics of the composite remarkably, leading to greater sensitivity and selectivity in terms of CAP detection. The MoN@S-GCN-modified electrode was characterized by an extremely low limit of detection (LOD) and wide linear working range (WLR) which underlines its suitability as an alternative to the current methods of analysis costly, with low sensitivity and complexity of operation. Moreover, the sensor was really good in analyzing real samples with large recovery values, good storage characteristics and high interference resistance. These results validate the suitability of MoN@S-GCN composites to cost-effective and sensitive electrochemical sensing of pharmaceutical pollutants [85].

This study was aimed at the objective of deciding how the photocatalytic hydrogen evolution capability of graphitic carbon nitride (g-C_3N_4) can be optimized by co-doping with both sulfur (S) and potassium (K). Though pure g- g-C_3N_4 has been considered an attractive metal-free photocatalyst, because it is chemically robust and thermally stable, its photocatalytic performance is impaired by poor absorption of visible light and a short lifetime of photogenerated charge carriers. In order to overcome these limitations, it used molten salt-assisted treatment to enhance crystallinity and facilitate electron delocalization in g-C_3N_4 framework. The resultant S and K co-doped g-C_3N_4 had a phenomenal rate of hydrogen generation of 8.78 mmol g-1 h-1 with visual light irradiation (l > 420 nm) that was nearly 98 times faster than the untreated g-C_3N_4. Also, it reached the apparent quantum

efficiency (AQE) of 70% at 420 nm. Photoluminescence and photoelectrochemical studies established that concurrent S and K doping had a pronounced effect in increasing the charge carrier mobility and separation efficiency, close to those allowing photolysis. The paper confirms that molten salt treatment together with co-doping can be used as an effective approach to develop an advanced photocatalyst in the production of hydrogen in a sustainable manner [86].

Graphitic carbon nitride with its surface modified with sulfur (S-g-C_3N_4) was taken as a surface modulator of fluorine doped Tin oxide (FTO) electrodes to create a cost effective and efficient hydro-detection electrochemical sensor with hydrazine. Hydrazine, despite its extensive use in industries, is highly toxic, which makes it very dangerous to the environment and human beings. Traditional methods of detection, such as the chromatographic and spectrophotometric ones, can be quite costly, time-consuming, as well as complex in terms of the instrumentation. Similarly, the common disadvantages of traditional electrochemical sensors are lack of sensitivity, instability of the signal, and interference. In order to address these drawbacks, an S-g-C_3N_4 material without metal was produced and deposited onto the FTO substrates by doctor-blade technique. Electrochemical characterization on the basis of cyclic voltammetry (CV) and linear sweep voltammetry (LSV) showed that the S-g-C_3N_4/FTO electrode had a much higher current response and stronger sensitivity than pristine g-C_3N_4-modified electrodes. This study has shown that S- g-C_3N_4 is a promising and cost-effective compound to be used in the environmental electrochemical sensing platforms [87].

The paper gave an account of designing a new electrochemical sensor using sulfur-doped graphitic carbon nitride nanoflakes to selectively and sensitively detect $Pb2^+$ ions. The contamination of lead is of particular concern given the fact that it is likely to bioaccumulate thus leading to serious health consequences including neurological disorders, cognitive disabilities, and damage of essential body organs. Although traditional methods of analysis like inductively coupled plasma mass spectrometry and atomic absorption spectrometry are very accurate, they are normally costly, laborious and cannot be used in-site analysis. Even though electrochemical sensing has such strengths as simplicity, cheapness and high

sensitivity, most of the current sensors use expensive materials or well-complicated fabrication processes. In order to overcome these, S-g-C_3N_4 nanoflakes were prepared by using a one-pot procedure with melamine and ammonium sulfate as starting materials. It was observed that the incorporation of sulfur improved Pb^{2+} ion adsorption with the creation of S-Pb interactions, as well as increased the surface area, electrical conductivity, and optical characteristics. The resultant sensor had high sensitivity, selectivity, and overall electrochemical performance than most of the existing methods of Pb^{2+} detection [88].

This paper dwells on photocatalysis of semiconductors specifically hydrogen creation by splitting water, and organic pollutants decadence as a solution to energy deficiency and environmental pollution. Graphitic carbon nitride (g-C_3N_4) is one of the photocatalysts that are available, which is sensitive to visible light, chemically stable, and inexpensive in production. Nonetheless, there are inherent drawbacks, slow charge conduction, small surface area, and fast recombination of electron-hole pairs, which limit its real-life implementation. In order to overcome such problems, a wide range of modification methods, such as elemental doping, heterojunction, and structural engineering have been studied. The doping of the g-C_3N_4, especially sulfur, has proven to be one of the most efficient methods of improving the visible-light absorption and charge separation. This paper has used a new synthesis methodology, which included in situ sulfur doping and thermal oxidative etching of two-dimensional g-C_3N_4 nanosheets (2D-SCN). Such a strategy expanded the surface area significantly, enhanced the charge transportation properties and enhanced the efficiency of electron-hole separation, which resulted in enhanced photocatalytic performance. The prepared 2D-SCN photocatalyst was highly active in the degradation of phenol and hydrogen evolution under simulated solar light. The article is a major step forward in the creation of high-performance photocatalysts in the production of renewable energy and environmental remediation procedures [89].

The non-enzymatic glucose sensor has become a promising alternative to the enzyme-based biosensors because it has better stability in its operations, cheap production, and the speed at which they respond to different conditions. In

comparison to enzymatic sensors which are frequently afflicted with enzyme denaturation, short lifespan and costly manufacturing, non-enzymatic systems are more robust and less sensitive to surface contamination. Even though non-enzymatic sensors based on carbon nanotubes, transition metal oxides, or even noble metal nanoparticles have good sensitivities, more recently graphitic carbon nitride (g-C_3N_4) has been considered in electrochemical glucose sensors. Its usefulness is, however, hampered by low electrical conductivity and exposure to surface blockage. In an attempt to address these drawbacks, scientists have come up with a hybrid nanomaterial by combining nickel sulfide (NiS) with sulfur-doped g-C_3N_4 (S-g-C_3N_4). Subsequent NiS/S-g-C_3N_4 nanohybrid had much better electrocatalytic characteristics in glucose oxidation, resulting in the desired improvement of sensing profile. Electrodes made using this hybrid material performed better than most reported glucose sensors in the past with high potential of reliable and efficient glucose detection in the clinical diagnostics and environmental monitoring processes [90].

Graphitic carbon nitride (g-C_3N_4) is a carbon material that is reported to be the thermodynamically most stable form of carbon nitride at ambient temperature and has found extensive use as a catalyst support. In its use of g-C_3N_4 as a support material, it stabilizes the metal oxide and improves the catalytic activity of metal oxides towards the activation of peroxymonosulfate (PMS). It was demonstrated in earlier research that carbon-based materials can be used to activate persulfates, but the catalytic activity of such materials varies depending on the type of carbon material used. Although it has benefits, pure g-C_3N_4 has low ability of PMS activation. The recent results reveal that heteroatom insertion into the g-C_3N_4 framework contributes significantly to the catalytic activity of the compound, mostly due to an alteration in the electronic structure. It has been demonstrated that oxygen doping works especially well because it influenced redistribution of the electron density, whereas sulfur doping also exhibited considerable increases in the PMS activation efficiency. In addition, the addition of sulfur has been noted to add graphene-based materials as PMS activators and catalysts to g-C_3N_4 in water oxidation reactions. These findings demonstrate that heteroatom doping is a

promising approach that can be used to address the inherent drawbacks of pristine g-C_3N_4 in advanced oxidation reactions [91].

In a different investigation, graphitic carbon nitride hollow microspheres (SCNHM) were doped with sulfur and used as a photocatalyst in the oxidation of tetracycline (TC) by the electrochemical method using the visible-light source. Tetracycline antibiotics are reported to be extremely challenging to the environment because of their low biodegradability, high persistence, toxicity, and antibiotic resistance. Synthesized SCNHM photocatalyst had a hollow interior structure with ultrathin nanosheets, which was made by self-assembly then treated with high temperature sulfur. This novel design was successful in counteracting the weaknesses of bulk g-C_3N_4 including inadequate light absorption and high recombination rate of photogenerated charge carriers. The high specific surface area, an increased ability in the absorption of visible light and higher efficiency in charge separation, were added factors to the high photocatalytic activity of SCNHM. The SCNHM photocatalyst was found to be of much higher degradation efficiency when compared to bulk g-C_3N_4, sulfur-doped g-C_3N_4, and g-C_3N_4 hollow microspheres when used as a model pollutant. Moreover, the material had high stability, durability and high antibacterial property against Escherichia coli and Staphylococcus aureus, which indicates that the material can be used in sustainable water treatment [92].

A g-C_3N_4-based molecularly imprinted surface plasmon resonance (MI-SPR) sensor based on the detection of fenoxaprop-ethyl (FEN) residues in rice samples was developed with a rapid and sensitive detection. FEN is a popular pesticide used in managing tan spot disease in wheat and is normally regarded as less harmful to non-target organism. However, residual FEN in food products has been known to be a potential health hazard and hence there is a need to identify it using reliable and accurate detection methods. Molecular imprinting was used in this work to produce specific binding cavities that were specific to FEN molecules and SPR technology was used to detect them in real-time. The S-g-C_3N_4 compound produced through thermal polycondensation was chosen as the material of the sensor making as the compound has a good chemical stability, is non-toxic, and has good optical

and electrical characteristics. The artificial MI-SPR sensor was highly sensitive, selective and had good recovery rates thus being able to quantify FEN residues accurately in rice samples. Moreover, the sensor proved to be cost effective and environmentally friendly which is why it is an attractive opportunity to monitor food safety [93].

The development of gold nanoparticles (AuNPs) onto sulfur-doped graphitic carbon nitrite nanosheets (SCNN-AuNPs) was proposed as a new electrochemical sensing material in the detection of inorganic arsenic (iAs). Arsenic is a highly poisonous element and a carcinogen, and it is necessary to use sensitive and precise methods of detection. The typical methods of analysis tend to be expensive, cumbersome, and inapplicable to on-site analysis and are not always able to detect the various arsenic species; however, they are highly sensitive. In order to overcome such shortfalls, SCNN was synthesized with an environmentally friendly co-condensation strategy followed by ultrasonic exfoliation which can offer flexible and conductive support of gold nanoparticles. It was discovered that sulfur doping immensely increased the electrical conductivity of g-C_3N_4 and increased the adhesion between AuNPs and the support medium to achieve better catalytic stability and performance. The resulting AuNPs@SCNN heterostructure displayed significantly high electrochemical activity in the reduction of arsenic, compared to conventional gold-based electrodes [94].

The current research was aimed at addressing the intrinsic shortcomings of graphitic carbon nitride (g-C_3N_4), such as the lack of light absorption, high rates of charge recombination, and catalytic potential, to enhance the efficiency of graphitic carbon nitride in photocatalytic hydrogen evolution. The g-C_3N_4 material with a fixed number of sulfur, nitrogen-deficient and cyano-functionalized (SDCN) was synthesized in a two-step strategy. This method was used to create two defects' sites within the g-C_3N_4 structure through the incorporation of sulfur atoms, cyano functional groups, and nitrogen vacancies. The availability of cyano groups and vacant nitrogen sites boosted the absorption of visible light, enhanced active separation of the charge carriers generated by photogeneration, and offered plenty of active adsorption and activation sites to the molecules. The further optimization of the electronic structure, the extension

of the optical absorption, and the acceleration of charge transfer were further accomplished with the help of sulfur doping and increased the hydrogen evolution reaction (HER). DFT results proved that these changes lowered the energy barriers involved in HER and enhanced the efficiency of charge transport. The shortcomings of pristine g-C_3N_4 have been overcome with the dual-defect engineering approach to achieve much better performance of photocatalysis and stability and illustrate how S-doped, defect-engineered g-C_3N_4 can be used to produce hydrogen in a sustainable manner [95].

The use of sulfur-doped graphitic carbon nitride (S-g-C_3N_4) into polysulfone (PSf) ultrafiltration membranes has been explored as one of the desired mechanisms of enhancing membrane performance. Even though ultrafiltration has found extensive use in different industrial industries, the application of ultrafiltration is usually limited due to membrane fouling and high-power consumption. Past attempts to solve the issue have been concerned with the addition of hydrophilic or metal-based additives but it is possible that the metal-based modifiers, when subject to long life cycle operation would leach, causing environmental issues and deterioration of performance. Graphitic carbon nitride (g-C_3N_4) has become a more sustainable material because of its naturally hydrophilic nature, porosity, chemical stability and harmless composition. It has a two-dimensional layered structure and has amine functionalities on its surface that allow easy functionalization and uniform dispersion in polymer matrices. Previous research has proven that g-C_3N_4 is capable of increasing the membrane characteristics of water flux, antifouling and mechanical strength. S-g-C_3N_4 in this paper was incorporated into PSf membranes through the phase inversion method that gave significant enhancements in the water permeability, separation and chemical stability. A more detailed structural and functional study also showed that the loading quantity of S-g-C_3N_4 was a key process affecting the membrane performance leading to the valuable information on designing robust and high-performing ultrafiltration membranes that may be used in the industry [96].

A good technique to identify diphenylamine (DPA), which is an antioxidant that is widely used in preserving fruits and has potential carcinogenicity has been introduced in this paper. Traditional methods of analysis like high-performance liquid

chromatography (HPLC) and gas chromatography (GC) though correct are usually costly and time-consuming. On the contrary, electrochemical sensing provides more affordable and less complicated alternative. The researchers came up with a new nanocomposite, which is abbreviated as SrPO/SCN that is comprised of a sulfur-doped graphitic carbon nitride (SCN) loaded in needle-like strontium pyrophosphate (SrPO). A simple co-precipitation method was used to synthesize this nanocomposite and serve as a modifier on a glassy carbon electrode (GCE). The needle-shaped morphology made it perfect in terms of the increased electron and mass transport thus greatly increasing the electrocatalytic performance. The SrPO/SCN sensor with a sensor had an extremely low detection threshold of 0.009 mmol L-1 and very high selectivity and stability. Its effectiveness as shown in successful use in actual samples, such as apples and pears, showed high recovery rates, which shows it is appropriate in food safety monitoring in practice [97].

The study targets the development of an extremely selective and sensitive molecularly imprinted quartz crystal microbalance (QCM) sensor in detecting dimethoate (DIM), an organophosphorus pesticide that is commonly used in the production of apple crops and poses severe health risks to people such as cancer and neurological disorders. The QCM sensors have advantages over conventional methods of analysis such as chromatography and mass spectrometry, which tend to be complex to use on complex food matrices due to their sensitivity, reproducibility, and operational ease. The proposed sensor is based on the nanocomposite of the sulfur-doped graphitic carbon nitride (S-g-C_3N_4) and erbium molybdate (Er-Mo), which combines the high surface area and the stability of S-g-C_3N_4 with the catalytic properties of Er-Mo. Molecular imprinting was utilized, in developing nano-scale recognition cavities of a molecular specificity to DIM molecules, resembling a lock-and-key system. The developed sensor was shown to have a better selectivity, high recovery rates in apple juice samples, and higher catalysis efficiency than its single components, which proved that it is useful in an analysis of pesticide residues [98].

This paper explains the synthesis and the performance study of a phosphorus and sulfur co-doped graphitic carbon nitrate (P 0.3S 0.2-CN) photocatalyst in the degradation of tetracycline (TC) and the subsequent in-situ results of hydrogen peroxide. It also has

environmental issues due to large usage of tetracycline antibiotics as it is persistent, resistant to biodegradation and ineffective on the elimination process of the utilization of conventional treatment processes. They have thus thought of using advanced oxidation processes (AOPs) in their place. The separation of charge carriers, redox capability [98]and total photocatalytic activity of the P0.3S0.2-CN catalyst prepared by hydrothermal method has been significantly enhanced when phosphorus and sulfur are co-doped with P0.3S0.2-CN, as opposed to that of P0.3S0.2-CN. The rate of hydrogen peroxide-generation of the catalyst under visible-light irradiation was 28.6 mg L-1 h-1 and the TC removal efficiency was 87.3 percent compared to the same dopes (P0.5-CN and S0.4-CN). The outcomes of the analysis of the calculations using the method of the separation of charge density and density functional theory (DFT) confirmed that the co-doping increased the light absorption, charge separation, and catalysis, and this method of co-doping was valuable [99].

This paper intended to achieve improved features of photocatalysis in eliminating the emergent pollutants in water by designing a heterostructure between a sulfur-based covalent organic framework (COF) and graphitic carbon nitride (g-C_3N_4). The photocatalysis has obtained significant focus as an environmentally viable procedure in terms of eliminating pollution and harnessing solar energy. Despite the low bandgap (at around 2.7 eV), easy synthesis and the fact that it is metal-free, the high level of electron-hole recombination limits the use of g-C_3N_4. COFs, however, are highly chemical stable, have tunable electronic properties and are hydrolysis resistant. In this paper, a sulfur-containing COF was prepared through the use of the tri(4-formylphenoxy) cyanurate and naphthalene diamine with the help of polycondensation. Although the COF had good absorption in the visible light, hydrophobicity inhibited its photocatalytic capability in aqueous. The solution to this was by conjugating the COF to g-C_3N_4 through a microwave-assisted synthesis technique, which reduced the synthesis time by a significant amount of time and increased interfacial interaction. The resulting COF-CN heterostructure was found to be better because it exhibited high levels of photocatalytic activity advanced through the combined capabilities of g-C_3N_4 to respond to the visible-light spectrum and COF to enable structural adaptation, a prospective water treatment application [100].

Carbon dioxide corrosion in the pipeline is a very important phenomenon in oil and gas industry because the compound reacts with water to produce carbonic acid, thereby increasing the rate of corrosion. Such an issue poses great economic, environmental and safety concerns in the form of higher maintenance expenses and the deterioration of infrastructure. Whereas the corrosion inhibitors are extensively used, the traditional inhibitors tend to be very costly, complicated chemically, and pose risks to the environment. This paper proposes a new alternative corrosion inhibitor, sulfur-doped graphitic carbon nitride (S-g-C_3N_4) as a cheap and sustainable substitute. S-g-C_3N_4 has good corrosion inhibition properties as it has a polymeric structure, an electron-rich surface, chemical stability, and easy functionalizability. Produced through a basic pyrolysis process, the substance is not toxic, simple to manufacture and structurally a versatile material. It is important to note that the use of S-g-C_3N_4 as a self-assembling corrosion inhibitor in aqueous conditions is reported in the first literature, which is a rather new and sustainable approach towards reducing CO_2-induced pipeline corrosion [101].

This paper underscores the increased attention to sulfur-doped graphitic carbon nitride (S-g-C_3N_4) as a potential photocatalyst in overcoming energy and environmental issues in the world. Graphitic carbon nitride is a graphene-like polymeric semiconductor that is appreciated because it is active in the visible light, chemically robust, and can be tuned to exhibit electronic properties. But it has low surface area and quick recombination of photogenerated charge carriers, which are the limitations of its photocatalytic performance. Several methods of modification have been considered to address these limitations, sulfur doping being one of them that have yielded positive results. Incorporation of sulfur improves the absorption of visible light, increases the efficiency of charge separation, and increases the photocatalytic activity by a significant margin. Consequently, S-g-C_3N_4 has shown superior performance in areas like reduction of CO_2, decomposition of pollutants as well as hydrogen generation. There are also some considerations on how to construct heterojunctions based on the use of S-g-C_3N_4 to enhance even more the transfer of charges and the photocatalytic performances. Although significant advances have been made, it is still difficult to maximize synthesis procedures and comprehend the mechanism behind the reaction,

so further studies are necessary to increase the number of practical uses of S-g-C_3N_4-based photocatalysts [102].

Yan and Cai (2021) examined how to prepare metal-lignin nanocomposites via the chemical coprecipitation procedure and thoroughly examined the challenges involved in the process that impact the quality and safety of the composite. The paper has shown that the functional groups of lignin allowed the coordination of the different metal ions but the coprecipitation process of metal was very sensitive to the reaction conditions, including the type of metal, solvent system, temperature, and concentration. It was noted that some metals, especially iron and copper, caused exothermic and Fenton-like reactions during coprecipitation resulting in quick release of heat and release of gases that presented serious safety issue and did not readily scale. Conversely, other metals like nickel demonstrated more stable reactions with lignin and hence produced relatively uniform composites with no serious side reactions. The authors found that despite the simplicity and low cost of coprecipitation in the production of metal-lignin nanocomposites it was necessary to carefully control the process parameters and have a complete understanding of the interactions between the metals and the lignin in the production of nanocomposites to ensure the consistency, safety, and successful dispersion of the metal species within the lignin matrix [103].

In the research by Yan and Cai (2020), the impact of various solvents on the preparation of Fe-lignin precursors to produce graphene-based nanostructures was studied in which kraft lignin was dissolved in the water, methanol, acetone, or tetrahydrofuran (THF) and then mixed with iron to form Fe-lignin composites, to be subjected to graphitization, and the authors measured the impact of the various solvents on the size of the particle, morphology, and performance of the synthesized nanoparticles [104].

A novel electrochemical sensor involving a graphite electrode coated with a kraft lignin@Ni@g-C_3N_4 nanocomposite to detect traces of the pesticide cypermethrin in drinking water was developed and evaluated in Journal of Materials Chemistry B with the nanocomposite synthesized by mixing graphitic carbon nitride with kraft lignin and nickel and was thoroughly characterized by FT-IR, PXRD, TEM, SEM, and EDX but drop-casted onto the electrode surface making the resulting sensor have a limit of detection ((LOD) of 0.026 $\mu g \cdot mL^{-1}$, well below regulatory limits for environmental

and food safety, indicating the material's effectiveness as a low-cost and sensitive alternative for pesticide monitoring [105].

Chapter 3
Materials and Methods

3.1 Materials:

All chemicals employed in this study were of analytical grade and used as received without any further purification. Kraft lignin was extracted from locally sourced bagasse. Ferric (III) nitrate nonahydrate ($Fe(NO_3)_3 \cdot 9H_2O$), thiourea (CH_4N_2S), hydrogen peroxide (H_2O_2, 30%), and melamine ($C_3H_6N_6$) were acquired from Sigma-Aldrich. n-Hexane and acetonitrile were used as solvents for preparing the model fuel. Dibenzothiophene (DBT, $C_{12}H_8S$) served as the sulfur-containing compound for evaluating oxidative desulfurization performance. All aqueous solutions were prepared using distilled water.

3.2 Preparation of Catalyst:

3.2.1 Extraction of kraft lignin (KL)

Kraft lignin was extracted from bagasse. Initially, 20 g of bagasse was mixed with 200 mL of distilled water and 1.66 mL of concentrated HCl and allowed to stand at room temperature for 24 h to promote acid hydrolysis. The mixture was then filtered to remove insoluble residues. The filtrate was treated with 3 g of NaOH dissolved in 3 mL of 30% hydrogen peroxide and diluted to 100 mL with distilled water. This solution was heated at 50°C for 30 min to facilitate partial oxidation and depolymerization of lignocellulosic components. After cooling, the pH was adjusted to approximately 4 using concentrated H_2SO_4, resulting in the precipitation of kraft lignin. The precipitate was collected, thoroughly washed with distilled water, and dried at 60°C. The extracted lignin was characterized using UV–Vis and FTIR spectroscopy to confirm its functional groups and structural integrity [106].

3.2.2 Synthesis of Fe@KL Nanoparticles

For metal incorporation, 5.55 mg of $Fe(NO_3)_3 \cdot 9H_2O$ was dispersed in 10 mL of distilled water and sonicated to obtain a homogeneous solution. Separately, 50 mg of extracted kraft lignin was dispersed in 50 mL of distilled water and sonicated for half an hour. Both solutions were stirred individually at room temperature for 2 h to ensure uniform dispersion. Subsequently, the iron precursor solution was added dropwise to the lignin dispersion and stirred for an additional 2 h to facilitate coordination between iron ions and lignin functional groups. The resulting mixture was aged at room temperature for 24 h to

promote stable complex formation. Finally, the product was dried at 60°C to obtain Fe@KL nanoparticles for further composite fabrication [104].

3.2.3 Synthesis of S@*g*-C_3N_4Nanoparticles

Sulfur-doped graphitic carbon nitride was synthesized using a thermal polymerization method. Thiourea (1.81 g) and melamine (1.0 g) were thoroughly mixed and placed in a covered alumina crucible. The mixture was calcined in a muffle furnace at 550°C for 5 h. During calcination, thiourea decomposed and supplied sulfur species that were incorporated into the g-C_3N_4 framework. After cooling, the yellow product was collected, ground into a fine powder, and stored for subsequent use [107]. This method ensures effective sulfur incorporation and structural uniformity, as reported in previous studies.

3.2.4 Fabrication of Fe@KL/S-g-C_3N_4 nanocomposite

To fabricate the composite catalyst, 18 mg of Fe@KL and 600 mg of S-g-C_3N_4 were dispersed in 40 mL of methanol and sonicated for 30 min to achieve uniform dispersion and enhanced interfacial interaction. The suspension was then employed in a reflux system and heated at 80°C under continuous stirring for 30 min, facilitating strong interaction between Fe@KL and the S@g-C_3N_4 matrix. After completion, the mixture was centrifuged, and washed several times with ethanol to remove unbound species [105]. The final product was dried at 110°C to obtain the Fe@KL/S@g-C_3N_4 nanocomposite, which was subsequently used for catalytic desulfurization studies.

3.3 Preparation of Model fuel

A model fuel was formed by dissolving 2 mg of DBT in 100 mL of n-hexane, resulting in a sulfur concentration of 200 ppm.

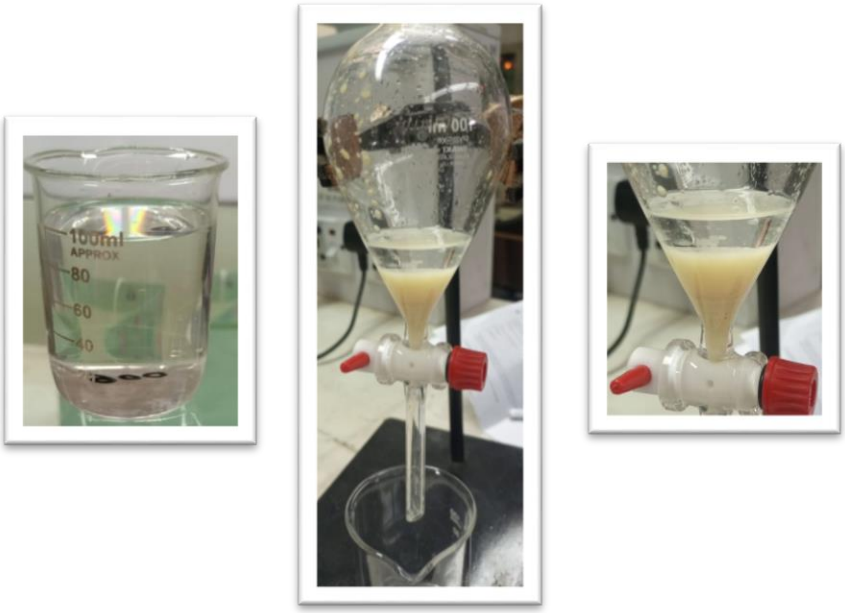

Figure 20. Model fuel and biphasic system of oxidative desulfurization.

3.3.1 Optimization of parameters for Photo-oxidative desulfurization

The photo-oxidative desulfurization experiments were conducted in a 50 mL flask while stirring. For each run, corresponding amount of the catalyst was added to 10 mL of the prepared model fuel, followed by the addition of 1 mL of hydrogen peroxide, which served as the oxidizing agent.

Prior to light exposure, the reaction mixture was stirred in the absence of light for 32.5 minutes to establish adsorption–desorption equilibrium between the catalyst surface and dibenzothiophene molecules. Subsequently, the suspension was irradiated with visible light using three tungsten lamps (200 W each) for an additional 32.5 minutes while maintaining constant stirring and a reaction temperature of 42.5 °C.

Upon completion of irradiation, 6 mL of acetonitrile was introduced into the reaction mixture and transferred to a separating funnel. The system was cooled to room temperature for 15 minutes, leading to the formation of two distinct phases: an upper oil phase and a lower acetonitrile phase. After photocatalytic oxidation, the layer containing the oxidized dibenzothiophene species was separated, and the remaining concentration of DBT was quantified using UV–visible spectrophotometry [108].

The DBT degradation efficiency was determined using Equation (ii):

$$\%conversion = \frac{C_i - C_0}{C_i} \times 100 \qquad \text{Eq (ii)}$$

where C_0represents the initial concentration of DBT, and C_i denotes the DBT concentration after photo-oxidative degradation.

Chapter 4
Results and Discussion

A variety of techniques, such as UV-Visible Spectroscopy (UV- Vis), Fourier Transform Infrared Spectroscopy (FT-IR), Raman Spectroscopy, X-ray Diffraction (XRD), Scanning Electron Microscopy (SEM), Energy-Dispersive X-ray Spectroscopy (EDX), and XPS were used to confirm the catalyst's successful synthesis.

4.1 FTIR Analysis

FTIR analysis was performed to investigate the surface functional groups and chemical interactions among Kraft lignin, S@g-C_3N_4, Fe@KL, and Fe@KL/S-g-C_3N_4 in the 4000–400 cm^{-1} range, as shown in Figure __. The broad absorption band appearing around 3400–3500 cm^{-1} corresponds to O–H and N–H stretching vibrations, indicating the presence of hydroxyl and amine groups, as well as adsorbed moisture on the material surface [109]. Peaks at approximately 2930 and 2833 cm^{-1} are attributed to aliphatic C–H stretching, characteristic of the lignin backbone [109].

The bands between 1600 and 1500 cm^{-1} represent aromatic C=C stretching vibrations, confirming the aromatic units present in both lignin and g-C_3N_4 frameworks [109, 110]. A distinct absorption band near 1620 cm^{-1} is associated with C=N stretching, while signals in the 1200–1300 cm^{-1} region correspond to C–N stretching vibrations of the heterocyclic heptazine rings in g-C_3N_4 [111]. The peak observed around 810–820 cm^{-1} can be assigned to triazine ring bending and C–S stretching modes, verifying the successful sulfur doping into the g-C_3N_4 lattice [110].

In Kraft lignin, characteristic bands at 1264 cm^{-1} and 1032 cm^{-1} correspond to guaiacyl units, while those at 1216 cm^{-1} and 1134 cm^{-1} indicate syringyl units [109]. In the Fe@KL and Fe@KL/S-g-C_3N_4 composites, additional peaks appearing around 560–600 cm^{-1} are assigned to Fe–O and Fe–O–C vibrations, confirming the successful coordination of Fe species with oxygen-containing groups in lignin [112]. These findings indicate strong interfacial interactions among Fe, lignin, and S-doped g-C_3N_4. It indicates that the nanocomposite has been synthesized without destroying the core structure of each component [112].

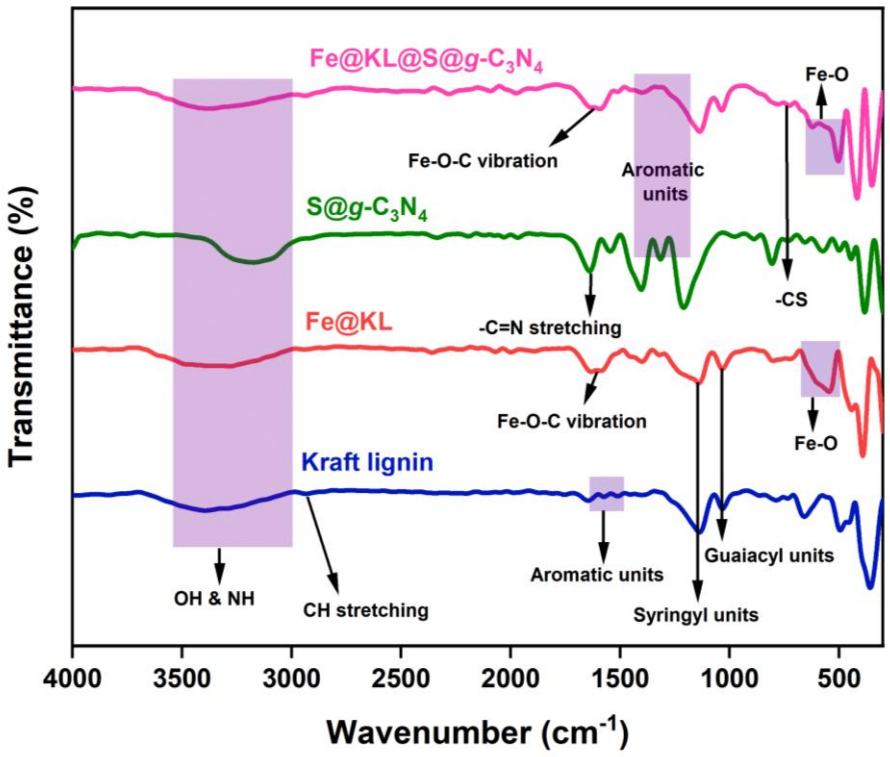

Figure 21. Comparison of FTIR spectrum of Kraft Lignin, Fe@KL, Sulfur doped g-C_3N_4 and Fe@KL/S-g- g-C_3N_4

Table 2. FTIR observed wavenumbers and functional group assignments

Functional Group Associated with Vibrations	Kraft Lignin	Fe@KL	S@g-C_3N_4	Fe@KL@S-g-C_3N_4
O–H & N–H stretching	3400–3200	–	–	–
C–H stretching	2930–2850	–	–	–
Aromatic units	1600, 1510	1600–1500	1600–1500	1600–1500
C=N stretching	–	–	~1650	–
Syringyl units	~1260	–	–	–
Guaiacyl units	1120–1030	–	–	–
C–S vibration	–	–	1100–1000	1100–1000
Fe–O–C vibration	–	1200–1100	–	1200–1100
Fe–O vibration	–	590–560	–	590–560

4.2 RAMAN Analysis

Raman spectroscopy was conducted to investigate the structural and bonding characteristics of Fe@KL, S@g-C_3N_4, and Fe@KL/S-g-C_3N_4 composites, as shown in Figure __. The characteristic bands observed around 973 cm^{-1} and 1153 cm^{-1} correspond to the in-plane bending of the heptazine motif and $–NH_x$ vibrations, respectively, confirming the polymeric network structure of g-C_3N_4 [113, 114]. The peaks near 1378 cm^{-1} (D band) and 1553 cm^{-1} (G band) are attributed to the disordered carbon and graphitic carbon structures, respectively, indicating the coexistence of amorphous and graphitic domains [114]. Furthermore, the broad bands located around 1630 cm^{-1} are associated with C–N and N=C=N stretching vibrations, which verify the presence of nitrogen-rich conjugated systems within the g-C_3N_4 framework [113, 115].

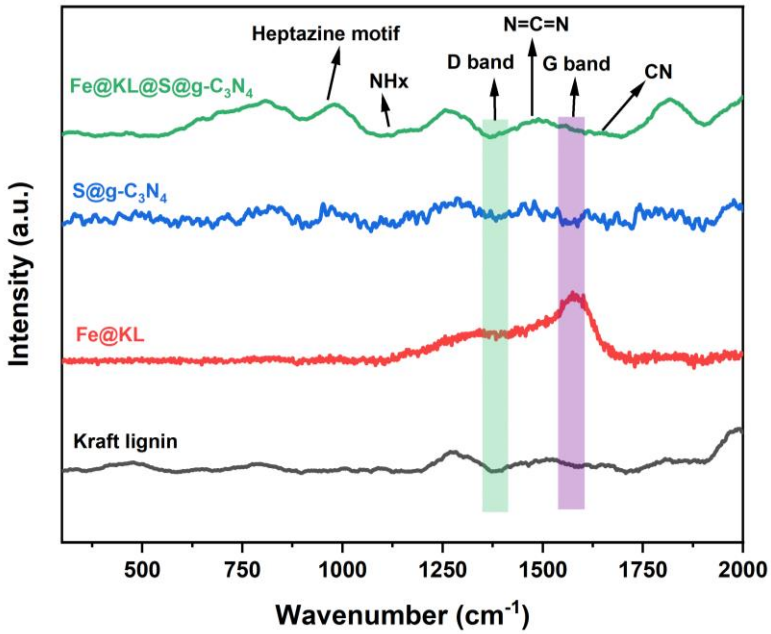

Figure 22. Comparison of Raman spectrum of Kraft Lignin, Fe@KL, Sulfur doped g-C_3N_4 and Fe@KL/S-g-C_3N_4.

The Fe@KL/S-g-C_3N_4 composite shows slightly enhanced D-band intensity compared to S@g-C_3N_4, suggesting that the incorporation of lignin and Fe species induces more structural disorder and defect sites [114]. These defect-rich regions are known to promote charge separation and provide additional active sites for catalytic reactions, thereby enhancing photocatalytic performance [116, 117].

4.3 UV-Vis Studies

The spectral characteristics of Kraft lignin, S-doped g-C3N4, and the Fe@KL, S-

g-C_3N_4 and the composite in the UV-Vis regime have characteristic absorption features which are indicative of their electronic structures. Kraft lignin exhibits a high absorption band at approximately 290 nm, which is a resultant characteristic p-p transitions of its aromatic rings and conjugated lignocellulosic phenolic groups, which are common to lignocellulosic biopolymers [1]. Conversely, g-C_3N_4 doped with sulfur exhibits a red-shifted absorption edge at approximately 320 nm, which possibly occurs due to the heteroatom incorporation of sulfur that distorts the heptazine structure, creates impurity states and improves n-p transitions [118]. These changes are useful in reducing the bandgap and enhancing visible-light absorbability.

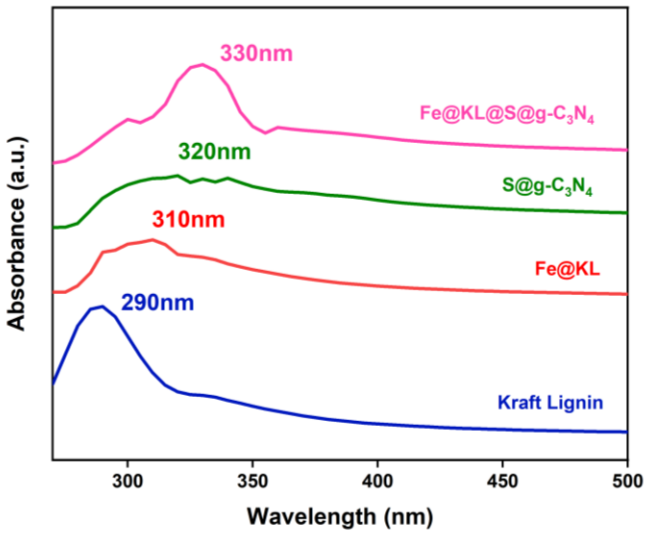

Figure 23. UV-vis absorbance spectra of KL, Fe@KL, S@g-C_3N_4 and Fe@KL/S-g-C_3N_4

The Fe@KL/S-g-C_3N_4 also increases the absorption edge to 330 nm, which is a result of a synergistic response between Fe, lignin and S-doped carbon nitride. The metalation-nitrogen and lignin-Fe chelation facilitates charge transfer and forms other localized states in the band structure, which enhance optimal harvesting efficiency [119]. The fact that the absorption tail is broadened is in line with the existence of intermolecular charge-transfer complexes and the occurrence of defect-mediated transitions.

$$\alpha h\upsilon' = A\,(h\upsilon' - E_{opt})^{n} \qquad \text{Eq. (ii)}$$

Planck's constant is represented by h, the photon frequency is indicated by υ', and the absorption constant is represented by A. Where the straight lines cross the axis at $(\alpha h\acute{\upsilon})^2=0$ yields the optical band gap values in the diagrams below [120]. According to Tauc plots drawn using the direct-transition models, one finds that Kraft lignin has a bandgap of 3.57 eV, consistent with wide-bandgap aromatic biopolymers [1]. The bandgap of S-doped g-C_3N_4 is also much reduced, and it is approximately 2.38 eV, which is similar to the sulfur-modified carbon nitride that had been reported before [118, 121]. Surprisingly, further reduction in the bandgap of Fe@KL@S-g-C_3N_4 composite to 1.85 eV is due to intense electronic interaction between Fe sites, lignin functional groups, and the g-C_3N_4 matrix. This interaction enables energy-effective charge delocalization, increases electron mobility and shifts the absorption to the visible spectrum to create a strong red-shift [119, 121].

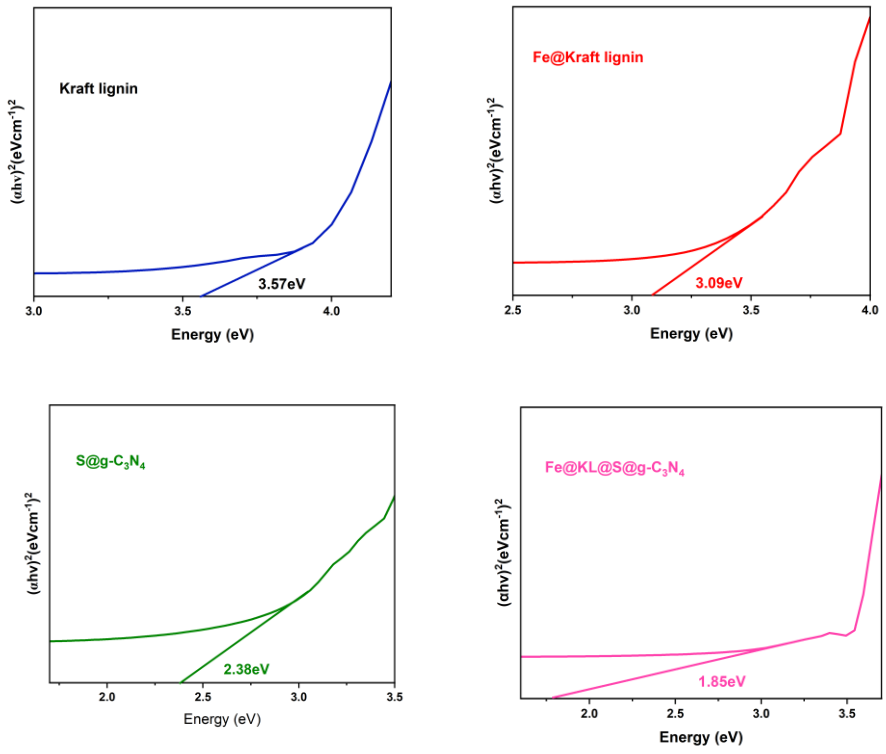

Figure 24. Figure 24. Band gap energies of KL, Fe@KL, S@g-C3N4 and Fe@KL/S-g-C3N4

In general, both UV- Vis and band-gap outcomes prove that the incorporation of Fe and lignin in S-doped g-C_3N_4 adjusts its electronic transitions, creates new energy

levels, and enhances its light-harvesting ability -important properties of visible-light-driven photocatalysis.

4.4 XRD studies

The X-ray diffraction patterns of Kraft lignin, Fe@KL, S-g-C_3N_4, and the Fe@KL/S-g-C_3N_4 composite reveal a clear structural evolution upon successive modification and hybridization. Kraft lignin exhibits a broad diffraction halo centered at approximately 18.9° (2θ) [122, 123], confirming its predominantly amorphous nature arising from randomly oriented aromatic units and the absence of long-range crystalline order, which is consistent with previous reports on technical lignin.

Upon iron incorporation, the Fe@KL sample shows additional low-intensity reflections at around 19°, 32°, 34°, and 48.9° (2θ), which can be attributed to poorly crystalline iron oxide species dispersed within the lignin matrix. These peaks correspond well with characteristic planes of hematite (α-Fe_2O_3) [124], in agreement with the standard JCPDS card No. 33-0664, where reflections near 33.2°, 35.6°, and 49.5° are commonly reported. The broad and weak nature of these peaks suggests nanoscale iron oxide domains and strong interaction between Fe species and the amorphous lignin framework rather than the formation of bulk crystalline iron oxides. T

he XRD pattern of S-g-C_3N_4 displays two characteristic diffraction peaks at approximately 13.3° and 27° (2θ), corresponding to the (100) and (002) planes of graphitic carbon nitride, respectively. The peak at ~13.3° is associated with in-plane structural packing of tri-s-triazine units, while the intense peak at ~27° reflects interlayer stacking of conjugated aromatic layers [125, 126], in good agreement with the hexagonal g-C_3N_4 phase indexed to JCPDS card No. 87-1526 [127].

In the Fe@KL/S-g-C_3N_4 composite, the dominant diffraction peak at ~27° (2θ) is retained, indicating that the layered graphitic carbon nitride framework remains structurally intact after integration with iron-modified lignin. A weak feature near ~12.8° further confirms the presence of the (100) plane of g-C_3N_4. Notably, the diffraction signals corresponding to iron oxide phases become significantly suppressed or indistinct in the composite, implying high dispersion of Fe species

and their incorporation into the hybrid matrix rather than separate crystallite growth.

This reduction in crystallinity suggests strong interfacial interactions among Fe@KL and S-g-C_3N_4, leading to the formation of a structurally integrated composite [128]. Overall, the XRD results confirm the amorphous nature of lignin, successful incorporation of nanoscale iron species, preservation of the layered g-C_3N_4 structure, and effective formation of the Fe@KL/S-g-C_3N_4 hybrid material, which is desirable for catalytic applications.

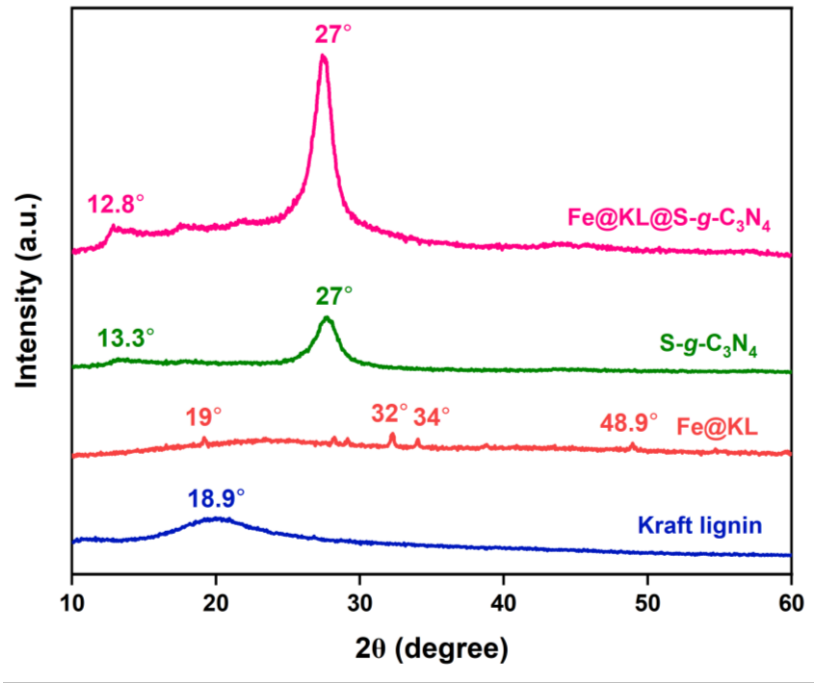

Figure 25. Analysis of XRD spectrum of Kraft Lignin Fe@KL, Sulfur doped g-$C_3N_4$and Fe@KL/S-g-C_3N_4.

4.5 SEM/EDX Studies

The morphology of the raw Kraft Lignin (KL) indicates the typically irregular and fragmented structure with smooth surfaces and broad distribution of the particle sizes. These heterogeneous aggregates are normally introduced by industrial Kraft lignin as precipitation process during wood delignification as is known in literature. Elemental analysis through EDX confirms that the major constituents are Carbon and Oxygen and there is significant content of the remaining Sulfur (usually 1-3 wt%), which is a chemical fingerprint of Kraft pulping process in which sodium sulfide has been used.

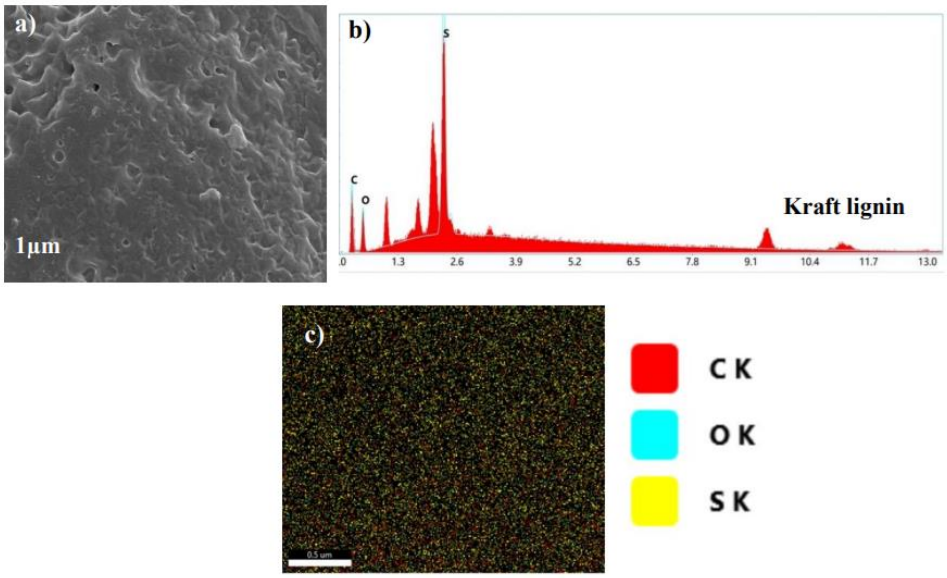

Figure 26. a) SEM image of Kraft Lignin; b) EDX spectrum of Kraft Lignin; c) Elemental mapping of Kraft lignin.

This standard morphology is known to be found in lignin powders [129] but recently, it was established that these are rounded and semi-spherical shapes in lignin powders using high-resolution SEM [130].

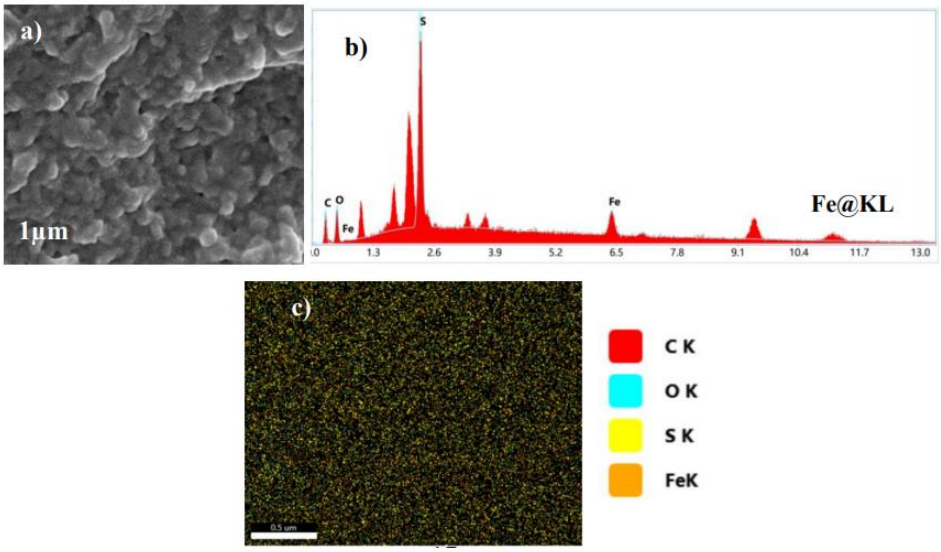

Figure 27. a) SEM image of Fe@KL; b) EDX spectrum of Fe@KL; c) Elemental mapping of Fe@KL.

When iron is added to create Fe@KL, a morphological change is observed in the lignin, with the smooth surfaces changed into rough and textured. The modification demonstrates the effective functionalization of iron species on the lignin matrix, probably due to the rich

presence of the hydroxyl and carboxyl functional groups that serve as coordination sites of the metal ions.

In the same manner, the S-C_3N_4 (Sulfur-doped carbon nitride) has a very different structure and is based on layered [131] and leaf-shaped, or wrinkled nanosheets. It is found in research that such S-doping results in a porous, fluffy structure in comparison to bulk carbon nitride [125].

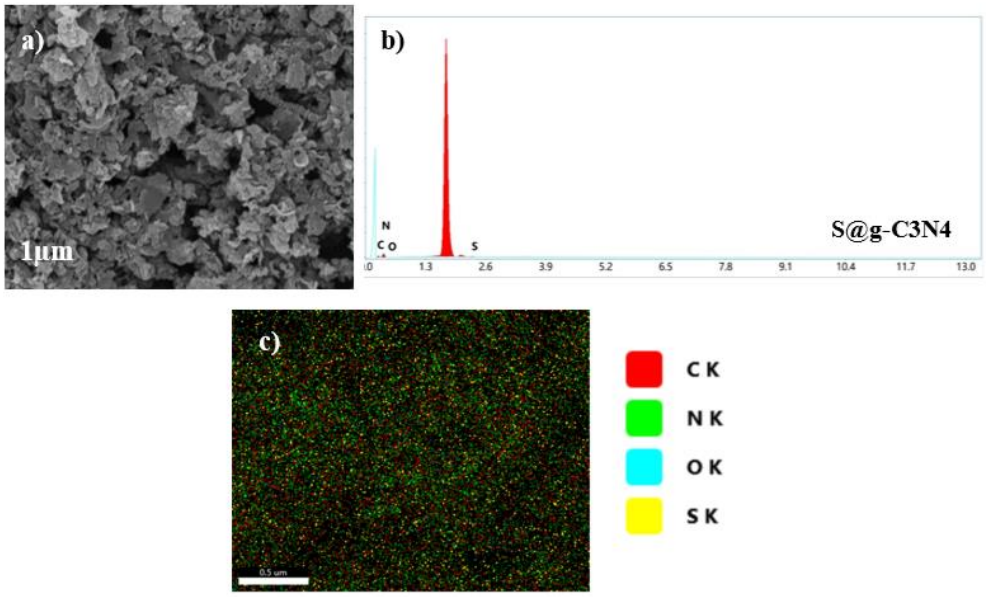

Figure 28. a) SEM image of S@g-C_3N_4; b) EDX spectrum of S@g- C_3N_4; c) Elemental mapping of S@g-C_3N_4.

The EDX mapping of this component indicates that there is even a distribution of Sulfur all over the nitrogenous framework which indicates that the sulfur atoms have been effectively incorporated into the lattice and not merely surface impurities.

Mixed with the carbon nitride nanosheets is a hierarchical heterostructure in which the lignin-iron particles are closely mixed with the sheets in the final integrated composite (Fe@KL/S-g-C_3N_4). Based on the images of the SEM, the S-g-C_3N_4 sheets are shown to surround or otherwise cover the modified lignin, and this surface-area interface is conducive to catalytic activity. This morphological synergy is comparable to the investigations by Zhang et al. (2025) who indicated that modified lignin can be properly etched and incorporated with sulfur-doped graphitic carbon nitrate to create stable and improved sensors and catalysts.

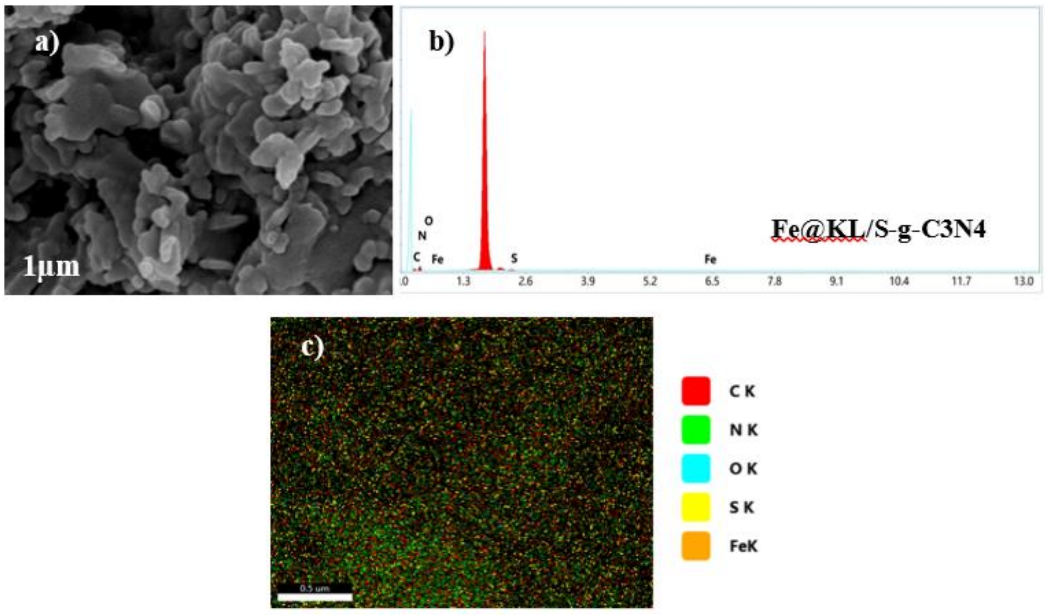

Figure 29. a) SEM image of Fe@KL/S-g-C_3N_4; b) EDX spectrum of Fe@KL/S-g-C_3N_4; c) Elemental mapping of Fe@KL/g-C_3N_4.

The integration is importantly evidenced in the elemental mapping of the composite, which indicates overlapping spatial distribution of Nitrogen, Iron, and Sulfur, and thus, it is clear that the two primary components have been united into a single material and not just a mere physical mixture.

The uniformity in the elemental maps that are seen under the microscope is fundamental to the desulfurization process as catalyst with a high density of active sites and a high transfer of electrons across the surface of the material. Moreover, the heterogeneous catalysis of the lignin proves that these morphological peculiarities, in particular, the hierarchical mixing of biopolymers with doped carbon structures, are the direct causes of the high efficiency of the oxidative desulfurization of fuels in mild conditions [132]

4.6 XPS Studies:

X-ray Photoelectron Spectroscopy was used to analyze the surface makeup and electronic condition of the resulting Fe@KL/S-g-C_3N_4 compound. The broad spectrum of the survey proves the presence of Carbon (C 1s), Nitrogen (N 1s), Oxygen (O 1s), Sulfur (S 2p) and Iron (Fe 2p) in the material.

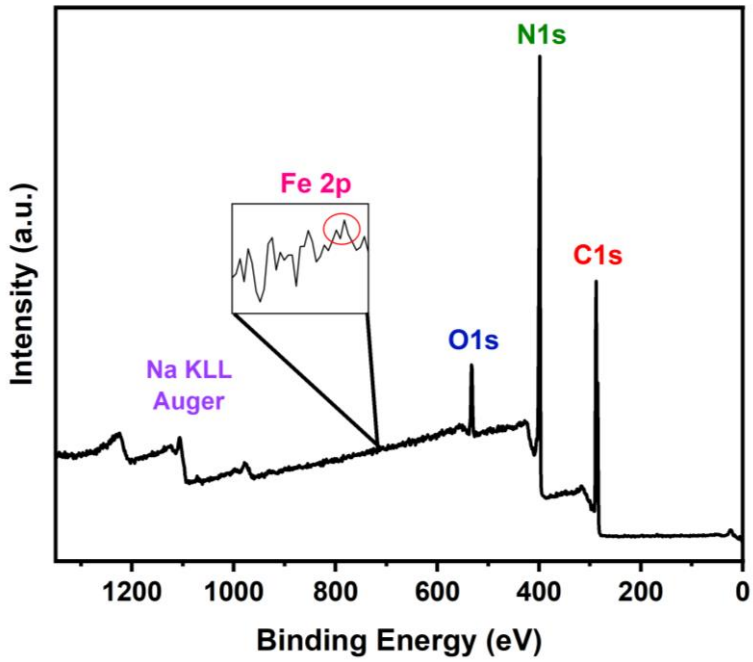

Figure 30. Broad survey spectrum of Fe@KL@S-g-C_3N_4.

The use of high-resolution C 1s spectra shows that the graphitic carbon in the triazine rings and lignin structure C-C/C=C and the carbon-oxygen bonds (C=O or O-C=O), respectively, are located at 284.8 eV and 288.4 eV, respectively [133].

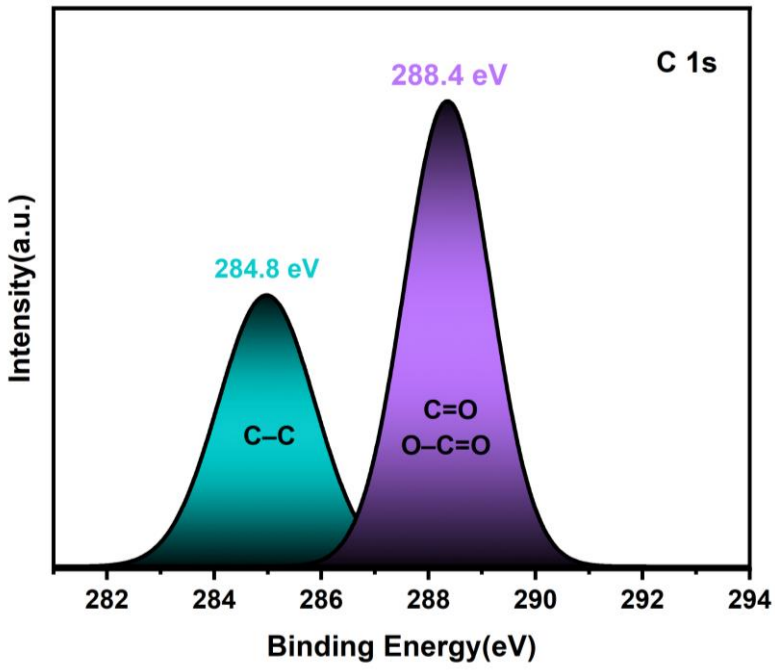

Figure 31. High resolution scan of C 1s.

The core-level spectrum of N 1s is deconvoluted into two major components of 398.8 eV and 400.1 eV, which are associated with the aromatic nitrogen (C=N-C) and tertiary nitrogen (N-$(C)_3$) present in the graphitic carbon nitride structure [133].

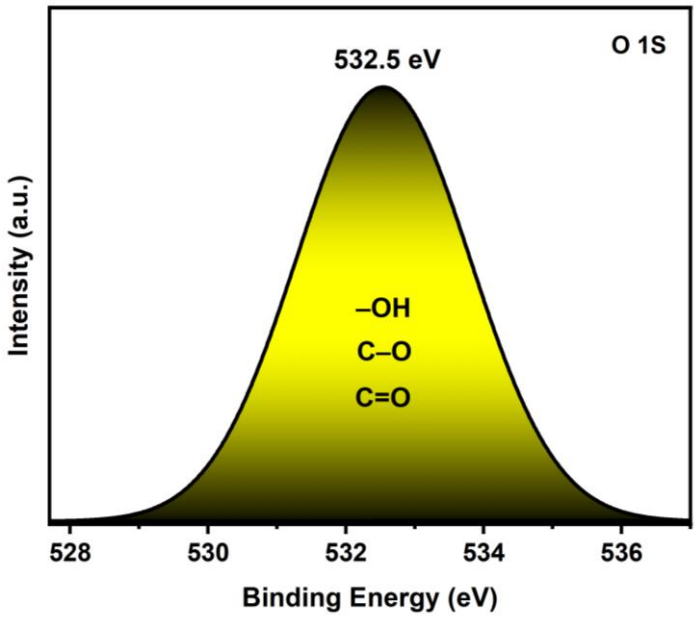

Figure 32. High resolution scan of O 1s.

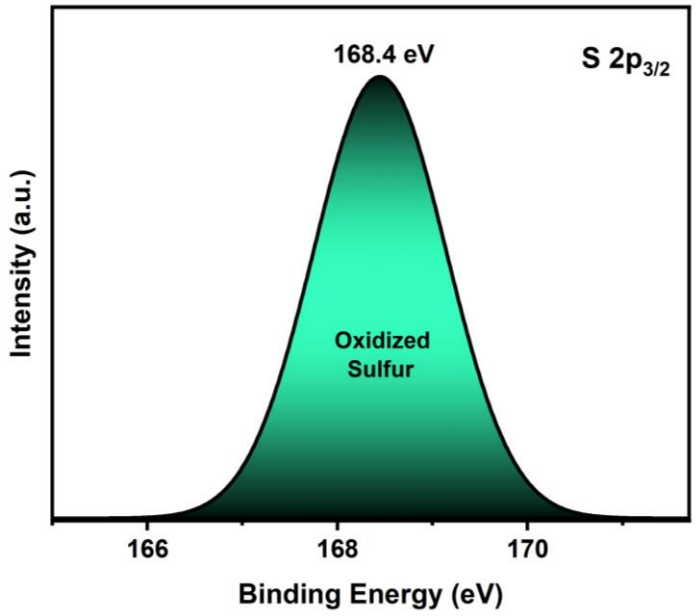

Figure 33. High resolution scan of S $2p_{3/2}$.

The O 1s spectrum which is centered around 532.5 eV represents the containing functional group of the lignin component such as -OH, C-O and C=O [134]. Most

importantly, the S 2p spectrum shows maximum at 168.4 eV, which means that oxidized SO_2 species exist in the compost [135].

Fe 2p high-resolution spectrum has a clear peak at 720.6 eV, which is identified to be the Fe^{3+} oxidation state and its satellite peak [136].

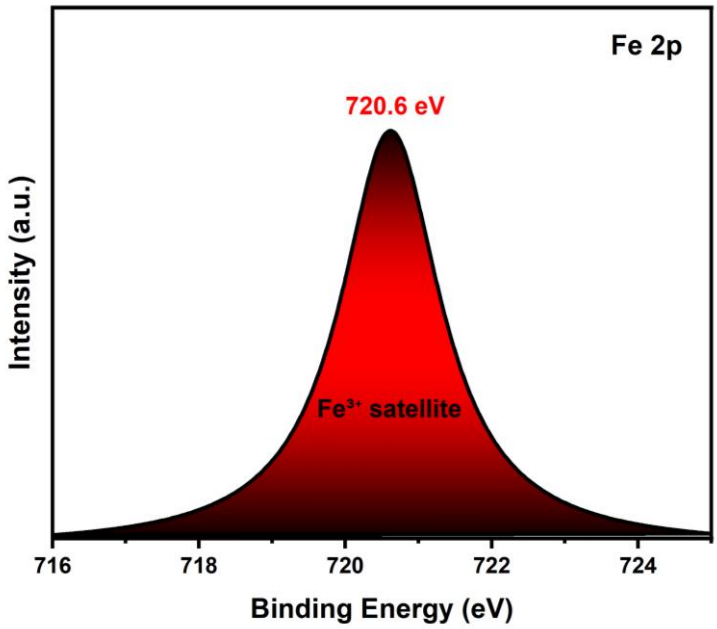

Figure 34. High resolution scan of Fe 2p.

Both Fe^{3+} and oxygen containing groups indicate that Fe-O coupled links have formed that are crucial in stabilizing the iron species through the interface.

A summary of comprehensive binding energies of the Fe@KL 0 -S- g-C_3N_4 composite is as follows:

Table 3. XPS binding energy values and chemical states of elements.

Element	Binding Energy (eV)	Key Assignment
C 1s	284.8 / 286.2 / 288.5	C–C/C=C, C–O, C=O/O-C=O
N 1s	398.6 / 400.1	C=N-C, N-(C)3 / –NH
O 1s	531.5 / 532.6	Fe–O/C=O, C–O/–OH
Fe 2p	710.9 / 724.4	Fe3+ (2p3/2, 2p1/2)

S 2p	163.4 / 164.6	C–S–C (2p3/2, 2p1/2)

4.7 Optimization using Response Surface Methodology

Response surface methodology was employed to degrade DBT with Box–Behnken design. In this statistical model, three independent variables were selected as critical parameters: catalyst dosage, reaction time, and reaction temperature. The Box–Behnken experimental design for the photo-oxidative desulfurization process consisted of a total of 17 experimental runs.

Table 4. Variables and their respective ranges and levels that impacted the desulfurization process.

Variables	**Range and levels**		
	-1	**0**	**1**
Catalyst dosage (g)	0.1	0.2	0.3
Reaction Time(minutes)	15	32.5	50
Reaction Temperature (℃)	25	42.5	60

Table 5. Experimental design matrix and observed desulfurization responses.

	Factor 1	**Factor 2**	**Factor 3**	**Response 1**
Run	**A:Catalyst Dosage**	**B:Temperature**	**C:Time**	**Desulfurization**
	g	℃	min	%
1	0.2	42.5	32.5	85.07
2	0.2	60	15	96.88
3	0.1	60	32.5	85.9

4	0.3	42.5	50	78.45
5	0.2	60	50	91.97
6	0.1	25	32.5	65.13
7	0.2	25	50	68.1
8	0.2	25	15	79.79
9	*0.1*	*42.5*	*50*	*60.67*
10	0.3	42.5	15	76.61
11	0.3	25	32.5	76.1
12	0.2	42.5	32.5	83.11
13	0.1	42.5	15	74.94
14	0.2	42.5	32.5	85.25
15	0.2	42.5	32.5	81.2
16	0.2	42.5	32.5	84.22
17	0.3	60	32.5	98.37

The response values span from 60.67 to 98.37, and the ratio of 1.59 indicates that no further adjustments are necessary.

4.7.1 Parametric conversion analysis of DBT in a Model fuel:

Regression analysis was employed to establish the relationship between the selected variables and the response, which was expressed in the form of a second-order polynomial equation, as presented in Equation (iii):

$$\text{Response (R)} = 83.77 + 5.36A + 10.50B - 3.63C + 37.50AB + 4.03AC + 1.70BC - 6.96A^2 + 4.56B^2 - 4.15C^2 \quad \text{eq. (iii)}$$

Among the various mathematical models evaluated by the software, including linear, two-factor interaction (2FI), cubic, and quadratic models, the quadratic model was found to provide the best fit to the experimental data. Consequently, the above equation was developed based on the quadratic model framework. To assess the adequacy of each model, Fischer's test (F-test) was performed by comparing the model error with pure experimental error. A model exhibiting a lower F-value is generally regarded as statistically more reliable. Since the calculated F-values for the linear, 2FI, and quadratic models exceeded the corresponding tabulated F-values at their respective degrees of freedom, the null hypothesis indicating a significant lack of fit was rejected [137].

4.7.2 Lack of fit and Model fit statistics

Table 6. Lack-of-fit analysis.

Source	Sum of Squares	df	Mean Square	F-value	p-value	
Linear	437.25	9	48.58	17.47	0.0072	
2FI	360.32	6	60.05	21.60	0.0052	
Quadratic	**4.70**	**3**	**1.57**	**0.5639**	**0.6671**	**Suggested**
Cubic	0.0000	0				Aliased
Pure Error	11.12	4	2.78			

Table 7. Summary statistics for model assessment.

Source	Std. Dev.	R^2	Adjusted R^2	Predicted R^2	PRESS	
Linear	5.87	0.7308	0.6687	0.4704	882.15	
2FI	6.09	0.7770	0.6432	-0.0049	1673.85	
Quadratic	**1.50**	**0.9905**	**0.9783**	**0.9444**	**92.65**	**Suggested**
Cubic	1.67	0.9933	0.9733		*	Aliased

The quadratic model was ultimately selected due to its higher polynomial order and superior performance in the model summary statistics. Furthermore, the aliased model was

excluded from consideration because of its comparatively lower coefficient of determination (R^2), whereas highest R^2 value was exhibited by the quadratic model exhibited the, confirming its suitability for accurately describing the experimental system.

4.7.3 Variance analysis (ANOVA) for Quadratic Model

Analysis of variance calculated the mean square values for each model term by using response surface methodology. It determined the corresponding degrees of freedom and sums of squares associated with the independent variables.

Table 8. Assumptions for ANOVA in the context of the Quadratic Model.

Source	Sum of Squares	df	Mean Square	F-value	p-value	
Model	1649.84	9	183.32	81.07	< 0.0001	significant
A-Catalyst Dosage	229.94	1	229.94	101.69	< 0.0001	
B-Temperature	882.00	1	882.00	390.07	< 0.0001	
C-Time	105.34	1	105.34	46.59	0.0002	
AB	0.5625	1	0.5625	0.2488	0.6332	
AC	64.88	1	64.88	28.70	0.0011	
BC	11.49	1	11.49	5.08	0.0588	
A^2	203.74	1	203.74	90.11	< 0.0001	
B^2	87.60	1	87.60	38.74	0.0004	
C^2	72.38	1	72.38	32.01	0.0008	
Residual	15.83	7	2.26			
Lack of Fit	4.70	3	1.57	0.5639	0.6671	not significant
Pure Error	11.12	4	2.78			

Cor Total	1665.66	16				

The F-value of 81.07 indicates the model is significant. There is a 0.01% chance that this value could occur due to noise.

P-values less than 0.0500 indicate model terms are significant. In this case A, B, C, AC, A^2, B^2, C^2 are significant model terms. Values greater than 0.1000 indicate the model terms are not significant. If there are many insignificant model terms (not counting those required to support hierarchy), model reduction may improve your model.

The Lack of Fit F-value of 0.56 means it is not significant relative to the pure error. There is a 66.71% chance that a Lack of Fit F-value this large could occur due to noise. Non-significant lack of fit is good.

Table 9. Metrics for Assessing Model Adequacy.

Std. Dev.	1.50	**R^2**	0.9905
Mean	80.69	**Adjusted R^2**	0.9783
C.V. %	1.86	**Predicted R^2**	0.9444
		Adeq Precision	32.9157

The Predicted R^2 of 0.9444 is very close to the Adjusted R^2 of 0.9783. Adeq Precision measures the signal to noise ratio. Our ratio of 32.916 this model can be used to navigate the design space.

The Predicted R^2 value of 0.9444 shows good agreement with the Adjusted R^2 value of 0.9783, as the difference between them is less than 0.2, indicating reliable predictive capability of the model. Adequate Precision, which evaluates the signal-to-noise ratio, yielded a value of 32.9157. Since a ratio greater than 4 is considered acceptable, this high value confirms that the model possesses a strong signal and is suitable for exploring the experimental design space.

The graphical comparison between the predicted and experimentally obtained DBT conversion efficiencies is illustrated in the corresponding figure. The plot demonstrates minimal deviation between the regression line, representing predicted values, and the experimental data points, confirming the robustness of the developed model. The coefficient of determination (R^2), which reflects the degree of correlation between experimental and predicted responses, was employed to assess the accuracy of the model

[137].

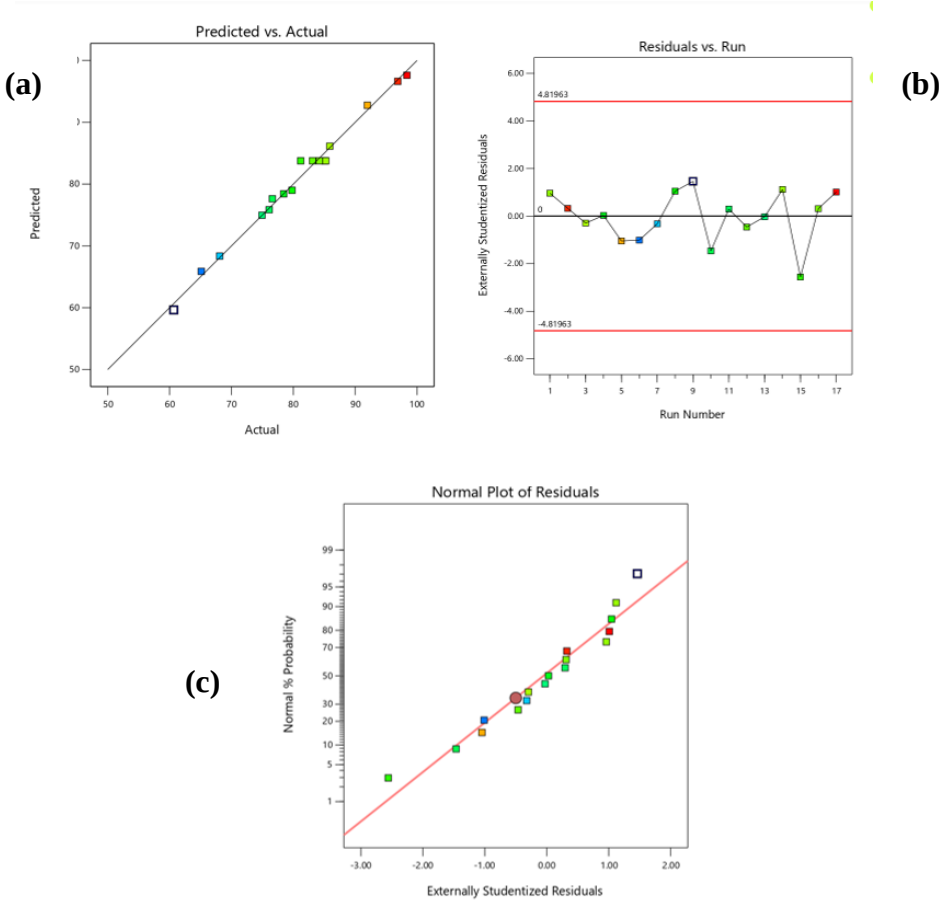

Figure 35. (a) Predicted vs actual responses of DBT conversion, (b) externally studentized against the run number, and (c) Normal % probability against externally studentized residuals.

Figure 4.6(a) presents a comparative analysis of predicted versus experimental DBT conversion percentages, showing only a negligible deviation from the regression line. Additionally, the validity of the model is further supported by the random dispersion of residuals around the reference line in Figure 4.6(b). The adequacy of the regression model was further examined through a normal probability plot of externally studentized residuals, as shown in Figure 4.6(c), which reveals a uniform distribution of residuals and confirms the statistical soundness of the model.

4.7.4 Analysis of Surface Contour plots and 3D graphs

The relationships between the independent variables and the response are visually represented through both 2D and 3D graphical techniques. The contour plot provides a two-dimensional projection of the reaction surface, illustrating how the response varies

across different combinations of experimental parameters. These plots identify the interaction between key points and help locate the optimal regions for the reaction. To provide a more

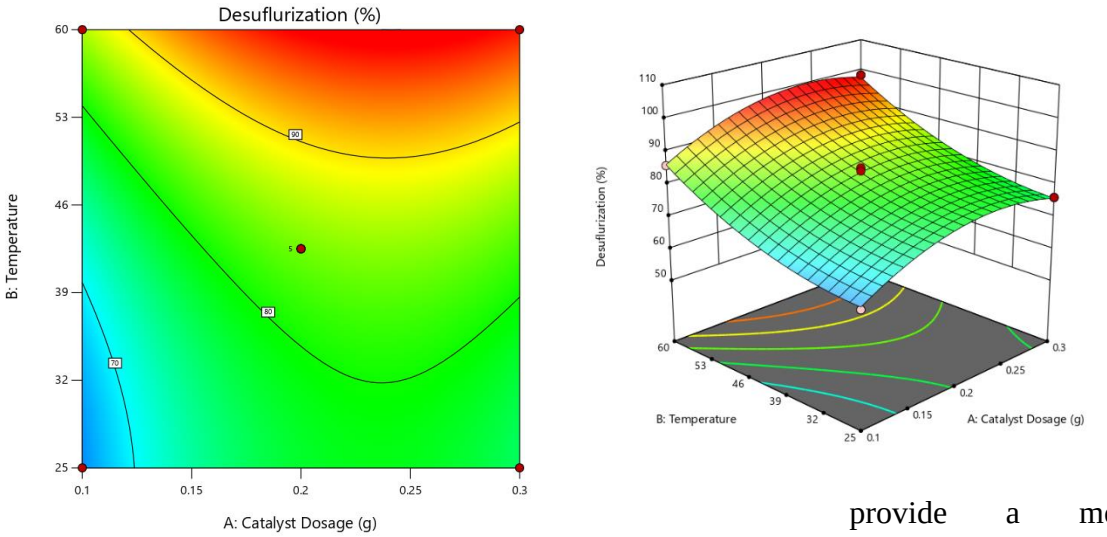

Figure 36. Contour plot and 3D graph illustrating the effect of temp and catalyst dosage.

comprehensive view, the 3D surface plot offers a three-dimensional perspective of the mathematical model. This visualization utilizes height and color gradients to emphasize the overall structure of the response surface. By combining these two perspectives, the interplay between parameters becomes more evident, allowing for a precise determination of the conditions required for maximum catalytic efficiency. The Fe@KL/S-g-C_3N_4 catalyst is used to desulfurize the model fuel. The ideal experimental parameters are 42.5°C, 0.3 g of catalyst, and 32.5 minutes of reaction time.

Figure 37 shows the relationship between temperature and catalyst dosage on the desulfurization activity of composite. It indicates that the desulfurization activity has its maximum 98.37 at about 46℃ and 0.20 g of catalyst. At higher doses of catalyst, the activity starts to exhibit a marginal decrease probably because of the occupation of active sites. Similarly, the activity is low at low temperature and dosage; the lowest activity of 70% was observed at 25℃ with the dosage of catalyst at 0.10 g. The activity of desulfurization slowly recuperates and levels off with an increase in temperature and the quantity of catalyst to the upper-right area of the graph.

Figure 31 shows the impact of the catalyst dosage and reaction time on the desulfurization activity of Fe@KL/S-g-C_3N_4 composite. The activity peaked at high local levels of about

85 at a catalyst dosage of about 0.20 g and a reaction period of 36 minutes. First, the desulfurization activity increases with increase in the dose of the catalyst and at minimum levels.

The activity though starts demonstrating slight diminution following the dosage more than 0.20 g, specifically at shorter reaction intervals. Moreover, with the extension of the reaction time, above 43 minutes, activity recovers greatly to occur even further and finally the result is a maximum 98.37% desulfurization with the reaction time being extended. This indicates that the quantity of catalyst and reaction time work dynamically to give maximum efficiency in the desulfurization over the tested range.

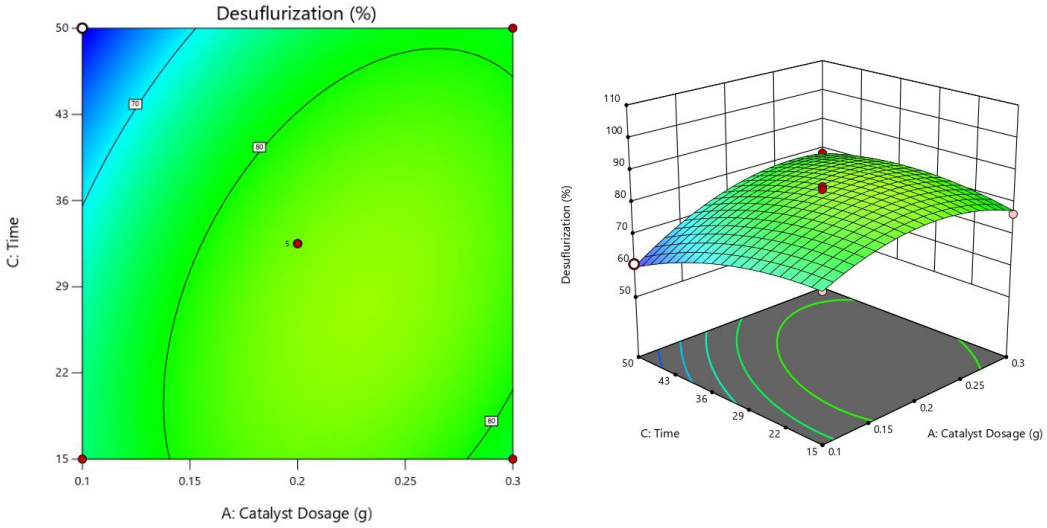

Figure 37. Contour plot and 3D graph illustrating the effect of time and catalyst dosage.

Figure 4.10 demonstrates the overall effect of reaction time and temperature on the desulfurization activity of Fe@KL/S-g-C_3N_4 catalyst. The catalytic activity at a moderate temperature of 46℃ and reaction duration of 36 minutes is positively correlated with reaction parameters with a localized maximum of approximately 85%. Conversely, much slower reaction times at low temperature cause a slow decline in efficiency with the activity reducing to about 70 percent at 25℃ and 15 minutes. Conversely, the activity is still strong and keeps on increasing with rise in temperature up to 60℃ in the presence of moderate reaction periods. Adhering to this pattern, the desulfurizing process steadily rises to its highest point of 98.37 percent with more time taken to react at these high temperatures.

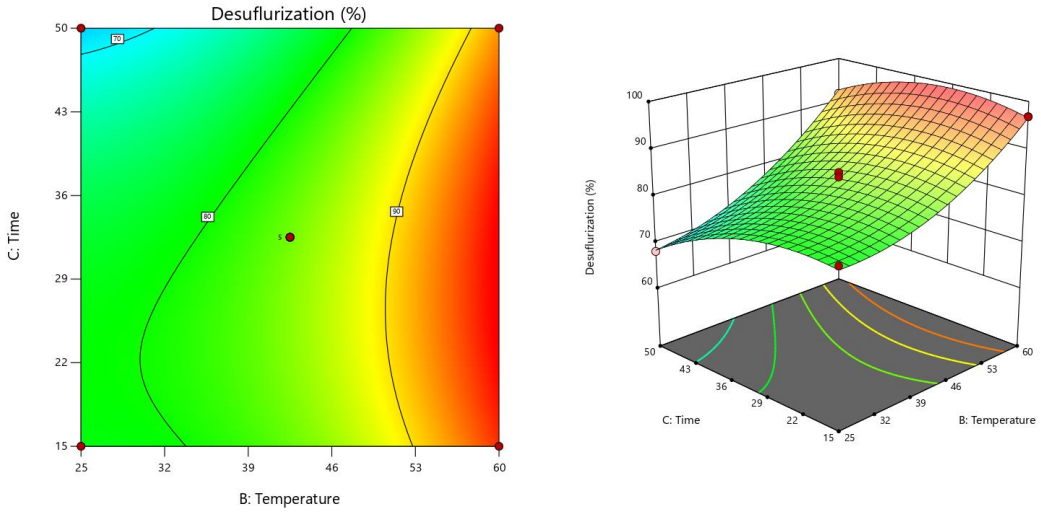

Figure 38: Contour plot and 3-dimensional graph illustrating the effect of time and catalyst dosage (C.D).

4.8 Recyclability of prepared catalyst

Recycling experiments were conducted to assess Fe@KL/S-g-C_3N_4 stability. With a slight modification in the last step, the testing process was comparable to the photocatalytic reaction tests. Following the complete breakdown of $DBTSO_2$, the leftover catalyst was gathered and utilized again to break down a fresh DBT sample that was made under the identical circumstances as the first one. Up to five cycles of this procedure were carried out. The catalyst's photocatalytic activity, which shown just a little drop throughout the first three cycles, demonstrated the stability of Fe@KL/S-g-C_3N_4 during these cycles as in Figure 34. The catalyst's long-term efficacy and endurance were demonstrated when it maintained up to 97% of its initial performance even after five successive cycles.

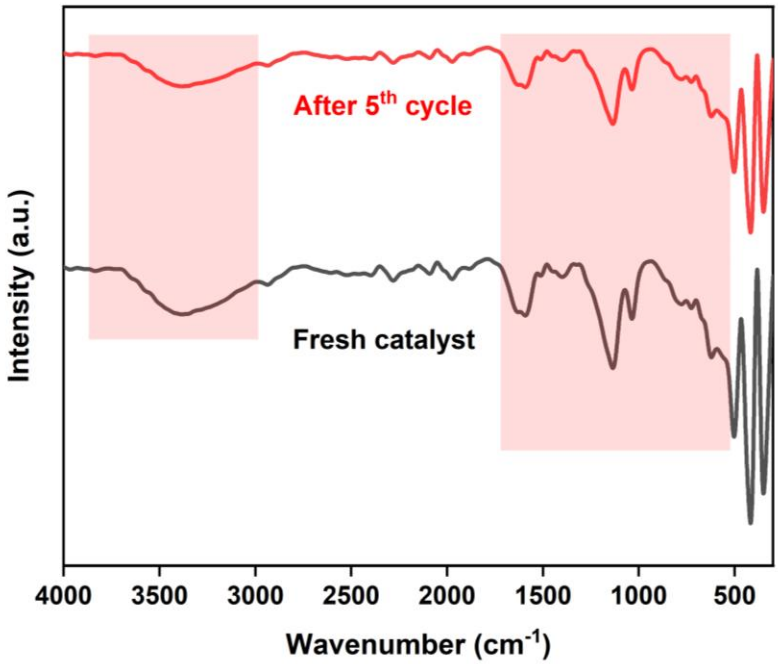

Figure 39. FT-IR spectra of both the fresh and reused catalysts.

The desulfurization activity gradually reduced throughout the cycle test, which is probably due to the accumulation of sulfone byproducts in the active sites. Based on these results, the catalyst exhibited an excellent stability, and cycle, and can be used in a prolonged continuous fashion [137].

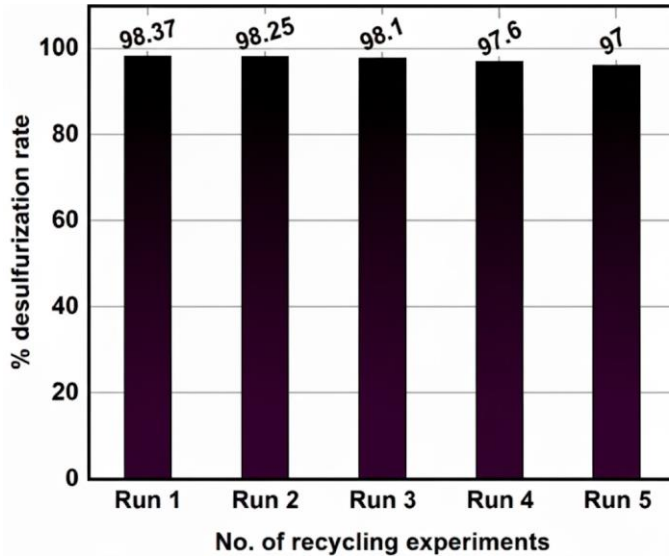

Figure 40. Reusability of the catalyst under ideal conditions.

Chapter 5
Conclusion

Model fuel PODS was investigated with hydrogen peroxide as the oxidant and Fe@KL/S-g-C_3N_4 as the catalyst. It was synthesized by the adsorption of Fe-doped kraft lignin onto the sulfur-doped g-C_3N_4 surface. To optimize the selectivity of sulfur conversion, the Box-Behnken design was applied to the investigation in terms of key factors: the amount of the catalyst, reaction temperature, as well as reaction time. The data have also indicated that the docking temperature of 42.5°C, the amount of the catalyst being 0.3 g and hydrogenation time 32.5 minutes offered the maximum desulfurization of DBT. The analysis of variance or ANOVA yielded a non-significant lack of fit of F= 0.5639 with an R^2 of 0.9951 on a quadratic model. Consequently, the sulfur concentration was reduced by 98.37% under these conditions. A great reusability was also observed with the catalyst being active for five cycles in terms of catalytic activities without appreciable deactivation. Due to its high efficiency and relatively low impact working conditions the PODS process can be the possible replacement for industrial fuel desulfurization.

References

1. Perkins, R.E.-E., H. *Fossil fuels 'stubbornly' dominating global energy despite surge in renewables: Energy Institute*. 2023; Available from: https://www.spglobal.com/energy/en/news-research/latest-news/crude-oil/062623-fossil-fuels-stubbornly-dominating-global-energy-despite-surge-in-renewables-energy-institute?
2. Petroleum), B.B., *BP Energy Outlook 2030*. 2012.
3. Organization, I.M., *IMO 2020 – cutting sulphur oxide emissions*. 2020.
4. Alzarqani, A.K. and F.J. Alduhaidahawi, *A study of sulfur content in crude oil, gasoline and Kerosene in Some Iraqi Oil Fields and Refineries.* International journal of health sciences, 2022. **6**(S4): p. 10548-10557.
5. Li, Y., *Health Disparities in the US and China: Spatial, Social, and Environmental Dimensions*. 2025: Taylor & Francis.
6. Organization, W.H., *Ambient (outdoor) air pollution*. 2024.
7. Nirmal Kumar, S., S. Appari, and B.V.R. Kuncharam, *Techniques for overcoming sulfur poisoning of catalyst employed in hydrocarbon reforming.* Catalysis Surveys from Asia, 2021. **25**(4): p. 362-388.
8. Song, C., *An overview of new approaches to deep desulfurization for ultra-clean gasoline, diesel fuel and jet fuel.* Catalysis Today, 2003. **86**(1): p. 211-263.
9. Kim, J.H., et al., *Kinetics of two pathways for 4, 6-dimethyldibenzothiophene hydrodesulfurization over NiMo, CoMo sulfide, and nickel phosphide catalysts.* Energy & fuels, 2005. **19**(2): p. 353-364.
10. Olindo, R. and J.G. Vogtländer, *The Role of Hydrogen in the Ecological Benefits of Ultra Low Sulphur Diesel Production and Use: An LCA Benchmark.* Sustainability, 2019. **11**(7): p. 2184.
11. Engineers, A.I.o.C., *The Relationship between Olefin Hydrogenation and Octane Number Loss in FCC Gasoline Hydrodesulfurization*. 2017.
12. Grokipedia, *Hydrodesulfurization*.
13. Zakzeski, J., et al., *The Catalytic Valorization of Lignin for the Production of Renewable Chemicals.* Chemical Reviews, 2010. **110**(6): p. 3552-3599.

14. Abin-Fuentes, A., et al., *Exploring the mechanism of biocatalyst inhibition in microbial desulfurization.* Appl Environ Microbiol, 2013. **79**(24): p. 7807-17.
15. Anbia, M. and S. Karami, *Desulfurization of gasoline using novel mesoporous carbon adsorbents.* Journal of Nanostructure in Chemistry, 2015. **5**(1): p. 131-137.
16. Juboori, S.A.-d.A. and G. Moradi, *Efficient Adsorptive Desulfurization of Dibenzothiophene Using Bimetallic Ni-Cr/ZSM-5 Zeolite Catalysts.* Catalysts, 2025. **15**(12): p. 1164.
17. Ghadiri, M., A. Ghaemi, and M. Shayanmehr, *A comprehensive review on exploring the potential and behavior of carbon-based adsorbents in the adsorptive desulfurization processes.* Fuel, 2026. **404**: p. 136222.
18. Srivastava, V.C., *An evaluation of desulfurization technologies for sulfur removal from liquid fuels.* Rsc Advances, 2012. **2**(3): p. 759-783.
19. Zhang, S., Q. Zhang, and Z.C. Zhang, *Extractive Desulfurization and Denitrogenation of Fuels Using Ionic Liquids.* Industrial & Engineering Chemistry Research, 2004. **43**(2): p. 614-622.
20. Zhu, Z., et al., *Deep eutectic solvents as non-traditionally multifunctional media for the desulfurization process of fuel oil.* Physical Chemistry Chemical Physics, 2021. **23**(2): p. 785-805.
21. Ahmad, M.S., et al., *Review of current technologies and future trends in ionic liquid-based systems for efficient desulfurization.* Separation and Purification Technology, 2025. **367**: p. 132690.
22. Hou, J., et al., *Sulfur metabolism in Rhodococcus species and their application in desulfurization of fossil fuels.* Journal of Applied Microbiology, 2023. **134**(3).
23. Nassar, H.N., et al., *Desulfurization of dibenzothiophene by a novel strain Brevibacillus invocatus C19 isolated from Egyptian coke.* Biosciences Biotechnology Research Asia, 2013. **10**(1).
24. Silva, T.P., et al., *Streamlining the biodesulfurization process: Development of an integrated continuous system prototype using Gordonia alkanivorans strain 1B.* RSC advances, 2024. **14**(1): p. 725-742.

25. Saha, B., S. Vedachalam, and A.K. Dalai, *Review on recent advances in adsorptive desulfurization.* Fuel Processing Technology, 2021. **214**: p. 106685.
26. Chen, L., et al., *Efficient oxidative desulfurization over highly dispersed molybdenum oxides supported on mesoporous titanium phosphonates.* Microporous and Mesoporous Materials, 2021. **315**: p. 110921.
27. Li, J., et al., *Heteropolyacids supported on micro/mesoporous materials PMoW@HKUST-1@ZSM-5-MCM-41: Effective catalyst for oxidative desulfurization with oxygen.* Molecular Catalysis, 2021. **504**: p. 111419.
28. Gao, Y., et al., *An Effective Hybrid Heterogeneous Catalyst to Desulfurize Diesel: Peroxotungstate@Metal–Organic Framework.* Molecules, 2020. **25**(23): p. 5494.
29. Abdollahi, M., et al., *Photocatalytic oxidative desulfurization of model fuel over visible light-active Cu-impregnated carbon-doped TiO2.* Journal of Cleaner Production, 2022. **380**: p. 134968.
30. Kasiri Baboukani, Z., A. Najafi Chermahini, and H. Farrokhpour, *Photocatalytic oxidative desulfurization of a model fuel using S-doped TiO2/BiVO4 composites: A combination of experimental and theoretical study.* Journal of Alloys and Compounds, 2024. **1002**: p. 175478.
31. Mitra, S., et al., *New insights on oxidative desulfurization for low sulfur residual oil production.* Sustainable Energy & Fuels, 2023. **7**(1): p. 270-279.
32. Syntyhaki, E., A. Detsi, and D. Karonis, *Assessment of the Oxidative Desulfurization of Middle Distillate Surrogate Fuels with Spectroscopic Techniques.* J Anal Methods Chem, 2020. **2020**: p. 8876082.
33. Flores, R., A. Rodas, and R. Gasperin, *Oxidative desulfurization of diesel fuel oil using supported Fenton catalysts and assisted with ultrasonic energy.* Petroleum Science, 2019. **16**(5): p. 1176-1184.
34. Yu, X., P. Han, and Y. Li, *Oxidative desulfurization of dibenzothiophene catalyzed by α-MnO 2 nanosheets on palygorskite using hydrogen peroxide as oxidant.* Rsc Advances, 2018. **8**(32): p. 17938-17943.
35. Tanimu, A., et al., *Metal-free catalytic oxidative desulfurization of fuels─ a review.* Energy & Fuels, 2022. **36**(7): p. 3394-3419.

36. Abdel-Maksoud, Y., E. Imam, and A. Ramadan, *TiO2 Solar Photocatalytic Reactor Systems: Selection of Reactor Design for Scale-up and Commercialization—Analytical Review*. Catalysts, 2016. **6**(9): p. 138.
37. Pei, J., et al., *Recent advances in g-C3N4 photocatalysts: A review of reaction parameters, structure design and exfoliation methods.* Catalysts, 2023. **13**(11): p. 1402.
38. Cao, S. and J. Yu, *g-C3N4-based photocatalysts for hydrogen generation.* The journal of physical chemistry letters, 2014. **5**(12): p. 2101-2107.
39. Bhanderi, D., P. Lakhani, and C.K. Modi, *Graphitic carbon nitride (gC 3 N 4) as an emerging photocatalyst for sustainable environmental applications: A comprehensive review.* RSC sustainability, 2024. **2**(2): p. 265-287.
40. Navarro, S., et al., *Literature Review on Graphitic Carbon Nitride (g-C3N4) as Photocatalyst for the Remediation of Water Polluted with Contaminants of Emerging Concern*, in *Preprints*. 2024, Preprints.
41. Bi, X., et al., *In-situ synthesis of g-C3N4 with nitrogen vacancy and cyano group via one-pot method for enhanced photocatalytic activity.* Scientific Reports, 2025. **15**(1): p. 19864.
42. Sudhaik, A., et al., *Review on fabrication of graphitic carbon nitride based efficient nanocomposites for photodegradation of aqueous phase organic pollutants.* Journal of Industrial and Engineering Chemistry, 2018. **67**: p. 28-51.
43. Pei, J., et al., *g-C3N4-Based Heterojunction for Enhanced Photocatalytic Performance: A Review of Fabrications, Applications, and Perspectives.* Catalysts, 2024. **14**(11): p. 825.
44. Khan, M.A., et al., *Recent advances over the doped g-C3N4 in photocatalysis: A review.* Coordination Chemistry Reviews, 2025. **522**: p. 216227.
45. Fan, Y., et al., *Graphitic carbon nitride for photocatalytic hydrogen production from water splitting: nano-morphological control and electronic band tailoring.* Nanomaterials, 2024. **15**(1): p. 45.
46. Chen, L., et al., *Phosphorus doped and defect modified graphitic carbon nitride for boosting photocatalytic hydrogen production.* Physical Chemistry Chemical Physics, 2023. **25**(1): p. 117-123.

47. Pérez-Torres, A.F., et al., *Sulfur-Doped g-C3N4 Heterojunctions for Efficient Visible Light Degradation of Methylene Blue.* ACS Omega, 2023. **8**(50): p. 47821-47834.
48. Lu, X.-J., et al., *Sulfur-doped gC 3 N 4 photocatalyst for significantly steered visible light photocatalytic H 2 evolution from water splitting.* Catalysis Science & Technology, 2024. **14**(3): p. 606-614.
49. Bi, L., et al., *Electron rich P doped g-C3N4 for photodegradation of 2,4-dichlorophenoxyacetic acid under visible light by improving oxygen adsorption: Performance and catalytic mechanism.* Separation and Purification Technology, 2023. **306**: p. 122562.
50. Singh, P.P. and V. Srivastava, *Retracted Article: Recent advances in visible-light graphitic carbon nitride (gC 3 N 4) photocatalysts for chemical transformations.* RSC advances, 2022. **12**(28): p. 18245-18265.
51. Xi, X., et al., *Flexible carbon-fiber/g-C3N4 nanosheet array as recyclable photocatalysts and photoelectrocatalysts.* Scientific Reports, 2025. **15**(1): p. 21090.
52. Ma, R., et al., *Intense interaction between biochar/gC 3 N 4 promotes the photocatalytic performance of heterojunction catalysts.* RSC advances, 2024. **14**(28): p. 19707-19717.
53. Ruan, Y., Y. Hu, and H. Cheng, *Recent Progress in g-C3N4-Based Photocatalysts for Organic Pollutant Degradation: Strategies to Improve Photocatalytic Activity.* Catalysts, 2025. **15**(2): p. 148.
54. Lu, Y., et al., *N3C-Defect-Tuned g-C3N4 Photocatalysts: Structural Optimization and Enhanced Tetracycline Degradation Performance.* Nanomaterials, 2025. **15**(6): p. 466.
55. Jiang, J., et al., *Dual defect sites at gC 3 N 4 synergistically induce the electron localization effect for boosting photocatalytic H 2 O 2 production.* Catalysis Science & Technology, 2024. **14**(22): p. 6701-6709.
56. Pérez-Torres, A.F., et al., *Sulfur-doped g-C3N4 heterojunctions for efficient visible light degradation of methylene blue.* ACS omega, 2023. **8**(50): p. 47821-47834.

57. Lin, T.-J. and C.-c. Chiu, *Influence of nonmetal dopants on charge separation of graphitic carbon nitride by time-dependent density functional theory.* Physical Chemistry Chemical Physics, 2020. **22**(2): p. 647-657.
58. Zhang, X., et al., *Photocatalytic oxidative desulfurization and denitrogenation of fuels over sodium doped graphitic carbon nitride nanosheets under visible light irradiation.* Materials Chemistry and Physics, 2019. **226**: p. 34-43.
59. Saeed, M., et al., *Facile Synthesis of a Novel Ni-WO(3)@g-C(3)N(4) Nanocomposite for Efficient Oxidative Desulfurization of Both Model and Real Fuel.* ACS Omega, 2022. **7**(18): p. 15809-15820.
60. Nilza, N. and M.D. Salam, *Recent advances in generation of bioproducts from lignin: a comprehensive review.* Discover Sustainability, 2025. **6**(1): p. 1083.
61. Mateo, S., G. Fabbrizi, and A.J. Moya, *Lignin from Plant-Based Agro-Industrial Biowastes: From Extraction to Sustainable Applications.* Polymers (Basel), 2025. **17**(7).
62. 42, I.B.T., *Sustainable Lignin Valorization*. 2021.
63. Gui, C., et al., *The catalytic valorization of lignin from biomass for the production of liquid fuels.* Energies, 2025. **18**(6): p. 1478.
64. Belluati, M., et al., *Biomass-derived carbon-based catalysts for lignocellulosic biomass and waste valorisation: a circular approach.* Green Chemistry, 2024. **26**(15): p. 8642-8668.
65. Branco, R.H., L.S. Serafim, and A.M. Xavier, *Second generation bioethanol production: on the use of pulp and paper industry wastes as feedstock.* Fermentation, 2018. **5**(1): p. 4.
66. Mattinen, M.-L., et al., *Colloidal lignin particles as adhesives for soft materials.* Nanomaterials, 2018. **8**(12): p. 1001.
67. Thakur, V.K. and M.K. Thakur, *Recent advances in green hydrogels from lignin: a review.* International journal of biological macromolecules, 2015. **72**: p. 834-847.
68. Ponnusamy, V.K., et al., *A review on lignin structure, pretreatments, fermentation reactions and biorefinery potential.* Bioresource technology, 2019. **271**: p. 462-472.

69. Dorrestijn, E., et al., *The occurrence and reactivity of phenoxyl linkages in lignin and low rank coal.* Journal of Analytical and Applied Pyrolysis, 2000. **54**(1-2): p. 153-192.
70. Milczarek, G., *Preparation and characterization of a lignin modified electrode.* Electroanalysis: An International Journal Devoted to Fundamental and Practical Aspects of Electroanalysis, 2007. **19**(13): p. 1411-1414.
71. Schutyser, W., et al., *Chemicals from lignin: an interplay of lignocellulose fractionation, depolymerisation, and upgrading.* Chemical society reviews, 2018. **47**(3): p. 852-908.
72. Jaimes-Paez, C.D., et al., *Sustainable synthesis of metal-doped lignin-derived electrospun carbon fibers for the development of ORR electrocatalysts.* Nanomaterials, 2023. **13**(22): p. 2921.
73. Zhai, G., et al., *Improved photocatalytic property of lignin-derived carbon nanofibers through catalyst synergy.* International Journal of Biological Macromolecules, 2023. **233**: p. 123588.
74. Sutradhar, S. and P. Fatehi, *Latest development in the fabrication and use of lignin-derived humic acid.* Biotechnology for Biofuels and Bioproducts, 2023. **16**(1): p. 38.
75. Alam, M.M., et al., *Efficient and environmentally friendly techniques for extracting lignin from lignocellulose biomass and subsequent uses: A review.* Cleaner Materials, 2024. **13**: p. 100253.
76. Makaveckas, T., A. Šimonėlienė, and V. Šipailaitė-Ramoškienė, *Lignin Valorization from Lignocellulosic Biomass: Extraction, Depolymerization, and Applications in the Circular Bioeconomy.* Sustainability, 2025. **17**(21): p. 9913.
77. Dubuisson, B., *EVALUATION OF LIGNIN PRETREATMENTS FOR IMPROVED FAST PYROLYSIS TO BIOAROMATIC COMPOUNDS*. 2019.
78. Zhu, C., et al., *Lignin-modified graphitic carbon nitride nanotubes for photocatalytic H(2)O(2) production and degradation of brilliant black BN.* Int J Biol Macromol, 2024. **267**(Pt 2): p. 131533.

79. Sandhu, Z.A., et al., *Response surface methodology: a powerful tool for optimizing the synthesis of metal sulfide nanoparticles for dye degradation.* Materials Advances, 2023. **4**(21): p. 5094-5125.
80. Hasanzadeh, R., et al., *Developing gasification process of polyethylene waste by utilization of response surface methodology as a machine learning technique and multi-objective optimizer approach.* International Journal of Hydrogen Energy, 2023. **48**(15): p. 5873-5886.
81. Hasanpour, M., et al., *Statistical analysis and optimization of photodegradation efficiency of methyl orange from aqueous solution using cellulose/zinc oxide hybrid aerogel by response surface methodology (RSM).* Arabian Journal of Chemistry, 2021. **14**(11): p. 103401.
82. Educator, T.O., *Box-Behnken Response Surface Methodology.*
83. R, S., *Optimising nanoparticles: harnessing quality by design through 3-level factorial design and box-behnken methodology.* International Journal of Pharmaceutics and Drug Analysis, 2024: p. 1-10.
84. Menezes, L., et al., *Solid-State Fermentation as a Green Technology for Biomass Valorization: Optimization Techniques for Bioprocess—An Overview.* BioEnergy Research, 2023. **17**: p. 1-17.
85. Ganesamurthi, J., et al., *MoN Nanorod/Sulfur-Doped Graphitic Carbon Nitride for Electrochemical Determination of Chloramphenicol.* ACS Sustainable Chemistry & Engineering, 2020. **XXXX**.
86. Chen, L., et al., *Sulfur and potassium co-doped graphitic carbon nitride for highly enhanced photocatalytic hydrogen evolution.* Applied Catalysis B: Environmental, 2020. **273**: p. 119050.
87. Mohammad, A., M.E. Khan, and M.H. Cho, *Sulfur-doped-graphitic-carbon nitride (Sg-C3N4) for low cost electrochemical sensing of hydrazine.* Journal of Alloys and Compounds, 2020. **816**: p. 152522.
88. Zou, J., et al., *Reliable and selective lead-ion sensor of sulfur-doped graphitic carbon nitride nanoflakes.* Applied Surface Science, 2020. **506**: p. 144672.

89. Lv, H., et al., *Synthesis of sulfur-doped 2D graphitic carbon nitride nanosheets for efficient photocatalytic degradation of phenol and hydrogen evolution.* ACS applied materials & interfaces, 2020. **12**(11): p. 12656-12667.
90. Vinoth, S., et al., *Nickel sulfide-incorporated sulfur-doped graphitic carbon nitride nanohybrid interface for non-enzymatic electrochemical sensing of glucose.* Nanoscale Advances, 2020. **2**(9): p. 4242-4250.
91. Wang, S., Y. Liu, and J. Wang, *Iron and sulfur co-doped graphite carbon nitride (FeOy/Sg-C3N4) for activating peroxymonosulfate to enhance sulfamethoxazole degradation.* Chemical Engineering Journal, 2020. **382**: p. 122836.
92. Bian, C., et al., *Enhanced photocatalytic activity of S-doped graphitic carbon nitride hollow microspheres: Synergistic effect, high-concentration antibiotic elimination and antibacterial behavior.* Journal of Colloid and Interface Science, 2023. **643**: p. 256-266.
93. Akıcı, Ş.Y., et al., *Fenpicoxamid-imprinted surface plasmon resonance (SPR) sensor based on sulfur-doped graphitic carbon nitride and its application to rice samples.* Micromachines, 2023. **15**(1): p. 6.
94. Ebrahimi, S., et al., *Self-supporting porous S-doped graphitic carbon nitride as a multifunctional support of Au catalyst: Application to highly sensitive and selective determination of arsenic (III) in a wide range of pH.* Electrochimica Acta, 2023. **437**: p. 141496.
95. Quan, Y., et al., *S-Modified graphitic carbon nitride with double defect sites for efficient photocatalytic hydrogen evolution.* Small, 2024. **20**(49): p. 2406576.
96. Vilakati, G.D., et al., *Probing the separation efficiency of sulfur-doped graphitic carbon nitride (g-C3N4)/polysulfone low-pressure ultrafiltration mixed matrix membranes.* Polymer Bulletin, 2023. **80**(8): p. 8759-8782.
97. Bhuvaneswari, C., et al., *Voltammetric nano-molar range quantification of agrochemical pesticide using needle-like strontium pyrophosphate embedded on sulfur doped graphitic carbon nitride electrocatalyst.* Food Chemistry, 2024. **437**: p. 137874.
98. Özdemir, N., et al., *A novel molecularly imprinted quartz crystal microbalance sensor based on erbium molybdate incorporating sulfur-doped graphitic carbon*

nitride for dimethoate determination in apple juice samples. Foods, 2024. **13**(5): p. 810.

99. Qin, L., et al., *Novel feathery P/S Co-doped graphitic carbon nitride for highly efficient synergistic photocatalytic H 2 O 2 generation and tetracycline degradation.* RSC advances, 2024. **14**(52): p. 38391-38402.
100. Zandipak, R., et al., *Synergistic effect of graphitic-like carbon nitride and sulfur-based thiazole-linked organic polymer heterostructures for boosting the photocatalytic degradation of pharmaceuticals in water.* Chemical Engineering Journal, 2024. **494**: p. 152843.
101. Anadebe, V.C., et al., *Sulfur-doped graphitic carbon nitride (Sg-C3N4) as an efficient corrosion inhibitor for X65 pipeline steel in CO2-saturated 3.5% NaCl solution: Electrochemical, XPS and Nanoindentation Studies.* Process Safety and Environmental Protection, 2022. **164**: p. 715-728.
102. Zuo, M., et al., *Modification of sulfur doped carbon nitride and its application in photocatalysis.* Separation and Purification Technology, 2023. **308**: p. 122875.
103. Yan, Q. and Z. Cai, *Issues in preparation of metal-lignin nanocomposites by coprecipitation method.* Journal of Inorganic and Organometallic Polymers and Materials, 2021. **31**(3): p. 978-996.
104. Yan, Q. and Z. Cai, *Effect of Solvents on Fe–Lignin Precursors for Production Graphene-Based Nanostructures.* Molecules, 2020. **25**(9): p. 2167.
105. Razzaque, S., et al., *Detection of toxic cypermethrin pesticides in drinking water by simple graphitic electrode modified with Kraft lignin@ Ni@ gC 3 N 4 nano-composite.* Journal of Materials Chemistry B, 2024. **12**(37): p. 9364-9374.
106. Joshi, K.M., et al., *Fragmented lignin-assisted synthesis of a hierarchical ZnO nanostructure for ammonia gas sensing.* RSC advances, 2019. **9**(5): p. 2484-2492.
107. Manoharan, K. and N.R. Krishna Chandar, *Hydrothermal Synthesis and Characterization of Sulfur-doped g-C3N4/VS4 nanocomposite for efficient photocatalytic applications.* Inorganic Chemistry Communications, 2023. **155**: p. 111047.

108. Zarrabi, M., M.H. Entezari, and E.K. Goharshadi, *Photocatalytic oxidative desulfurization of dibenzothiophene by C/TiO 2@ MCM-41 nanoparticles under visible light and mild conditions.* Rsc Advances, 2015. **5**(44): p. 34652-34662.
109. Faix, O., *Classification of lignins from different botanical origins by FT-IR spectroscopy.* 1991.
110. Xiao, X., et al., *One-step preparation of sulfur-doped porous gC 3 N 4 for enhanced visible light photocatalytic performance.* Dalton Transactions, 2020. **49**(24): p. 8041-8050.
111. Alaghmandfard, A. and K. Ghandi, *A Comprehensive Review of Graphitic Carbon Nitride (g-C(3)N(4))-Metal Oxide-Based Nanocomposites: Potential for Photocatalysis and Sensing.* Nanomaterials (Basel), 2022. **12**(2).
112. Zhao, D., et al., *Synthesis of Fe-Modified g-C3N4 Nanorod Bunches for the Efficient Photocatalytic Degradation of Oxytetracycline.* Materials, 2024. **17**(11): p. 2488.
113. Su, F., et al., *Structural distortion of g-C3N4 induced by N-defects for enhanced photocatalytic hydrogen evolution.* Catalysts, 2022. **12**(12): p. 1496.
114. Chusuei, C.C. and R.C. Nepal, *Role of defects and exposed graphene in carbon nanomaterial-based electrocatalysts.* New Journal of Chemistry, 2024. **48**(1): p. 260-267.
115. Maślana, K., et al., *Synthesis and Characterization of Nitrogen-doped Carbon Nanotubes Derived from g-C3N4.* Materials, 2020. **13**(6): p. 1349.
116. Yang, S., et al., *Carbon/C3N4 heterostructures constructed from lignin toward enhanced lithium-ion storage.* Carbon Research, 2024. **3**.
117. Lu, Q., J. Tai, and X. Song, *Preparation of cathode catalysts for efficient direct lignin fuel cells by nitrogen doping reduction of oxidized graphene with phthalocyanine iron and Kraft lignin.* Journal of Colloid and Interface Science, 2025. **677**: p. 983-993.
118. Ge, L., et al., *Enhanced visible light photocatalytic hydrogen evolution of sulfur-doped polymeric g-C3N4 photocatalysts.* Materials Research Bulletin, 2013. **48**: p. 3919-3925.

119. Pang, Y., et al., *Metal-doped carbon nitride: an all-in-one photocatalyst.* EES Catalysis, 2023. **1**(6): p. 810-831.
120. Xu, Y., et al., *Straightforward fabrication of lignin-derived carbon-bridged graphitic carbon nitride for improved visible photocatalysis of tetracycline hydrochloride assisted by peroxymonosulfate activation.* Advanced Composites and Hybrid Materials, 2023. **6**(6): p. 197.
121. Zhou, Z., et al., *Molecular engineering of polymeric carbon nitride: advancing applications from photocatalysis to biosensing and more.* Chemical Society Reviews, 2018. **47**(7): p. 2298-2321.
122. Kumari, S., et al., *New lignin-based polyurethane foam for wastewater treatment.* Rsc Advances, 2016. **6**(81): p. 77768-77776.
123. Butnoi, P., et al., *Electrospun nanocomposite fibers from lignin and iron oxide as supercapacitor material.* journal of materials research and technology, 2021. **12**: p. 2153-2167.
124. Hmamouchi, S., et al., *α-Fe2O3/g-C3N4 nanocomposite with type II heterojunction for methylene blue photodegradation.* Chemical Physics Impact, 2024. **8**: p. 100577.
125. Manoharan, K. and N.R.K. Chandar, *Hydrothermal Synthesis and Characterization of Sulfur-doped g-C3N4/VS4 nanocomposite for efficient photocatalytic applications.* Inorganic Chemistry Communications, 2023. **155**: p. 111047.
126. Alshammari, K., et al., *Synthesis of Sulfur@g-C(3)N(4) and CuS@g-C(3)N(4) Catalysts for Hydrogen Production from Sodium Borohydride.* Materials (Basel), 2023. **16**(12).
127. Yaqoubi, M., et al., *A novel ZnMn2O4/g-C3N4 nanocomposites heterojunction photocatalyst: preparation, characterization, and investigation of photocatalytic behavior over toxic dyes.* Applied Water Science, 2025. **15**(7): p. 172.
128. Xu, Y., et al., *Straightforward fabrication of lignin-derived carbon-bridged graphitic carbon nitride for improved visible photocatalysis of tetracycline hydrochloride assisted by peroxymonosulfate activation.* Advanced Composites and Hybrid Materials, 2023. **6**.

129. Shah, S.A., et al., *Sustainable oxidative desulfurization of fuel via lignin-derived heterogeneous catalysis: Optimized by Box-Behnken design for high efficiency under mild conditions.* Int J Biol Macromol, 2025. **310**(Pt 4): p. 143404.
130. Pua, F.L., et al., *Correction: Direct production of biodiesel from high-acid value Jatropha oil with solid acid catalyst derived from lignin.* Biotechnology for biofuels, 2011. **4**: p. 56.
131. Hajizadeh-Oghaz, M. and G. Heidari, *Synthesis and characterization of sulfur-doped g-C_3N_4 nanosheets for enhanced photocatalytic activity in the removal of organic pollutants.* Journal of Advanced Materials in Engineering, 2025. **45**(1): p. 33-48.
132. Savunthari, K.V., et al., *Green synthesis of lignin nanorods/g-C3N4 nanocomposite materials for efficient photocatalytic degradation of triclosan in environmental water.* Chemosphere, 2021. **272**: p. 129801.
133. Zhu, A., et al., *Interfaces of graphitic carbon nitride-based composite photocatalysts.* Inorganic Chemistry Frontiers, 2020. **7**(23): p. 4754-4793.
134. Madankar, R., et al., *Rapid synthesis of graphitic carbon nitride nanosheets as an efficient adsorbent for removal of Methylene Blue and Rhodamine B from Aqueous Solutions.* Sci Rep, 2025. **15**(1): p. 28999.
135. Scientific, T.F., *Sulfur X-ray photoelectron spectra, sulfur electron configuration, and other elemental information.*
136. Han, J., et al., *A hematite photoanode with gradient structure shows an unprecedentedly low onset potential for photoelectrochemical water oxidation.* Physical Chemistry Chemical Physics, 2014. **16**(43): p. 23544-23548.
137. Afzal, I., et al., *Logical Optimization of Metal–Organic Frameworks for Photocatalytic Degradation of Organic Pollutants in Water via Box–Behnken Design.* ACS ES&T Water, 2024. **4**(2): p. 648-660.

Turnitin Originality Report

Processed on: 09-Jan-2026 12:02 PKT
ID: 2854302227
Word Count: 20181
Submitted: 1

Desulfurization of Model Fuel Oil Using Modified Lignin@S-g-C3N4: Optimization via Response Surface Methodology By Saba Iqbal Ciit/sp24-r06-014/lhr

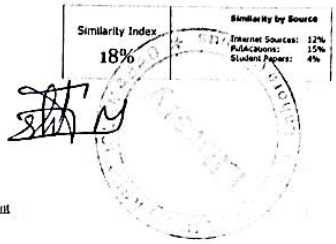

1% match (Internet from 13-Nov-2018)
https://pubs.acs.org/doi/10.1021/acs.chemrev.6b00075

1% match (Internet from 24-Feb-2025)
https://etul.aau.edu.et/server/api/core/bitstreams/3220b583-33b0-433e-9f3b-75ge3c58ea04/content

< 1% match (Internet from 12-Oct-2020)
https://www.mdpi.com/2073-4344/10/10/1119/html

< 1% match (Internet from 15-Jan-2024)
https://WWW.MDPI.COM/2079-4991/9/11/1507

< 1% match (Internet from 01-Jan-2026)
https://www.mdpi.com/2079-6374/15/5/315/xml

< 1% match (Internet from 01-Jan-2026)
https://www.mdpi.com/2079-4991/15/6/466/xml

< 1% match (Internet from 19-Jul-2024)
https://www.mdpi.com/1660-4601/21/7/914

< 1% match (Internet from 23-Dec-2025)
https://www.mdpi.com/2076-3417/15/14/8038

< 1% match (Internet from 31-Mar-2025)
https://www.mdpi.com/2073-4344/10/3/312

< 1% match (Internet from 01-Jan-2026)
https://www.mdpi.com/2079-4991/15/7/564/xml

< 1% match (Internet from 14-Jul-2025)
https://WWW.MDPI.COM/1420-3049/30/10/2137

< 1% match (Internet from 01-Jan-2026)
https://www.mdpi.com/2304-6740/13/4/118/xml

< 1% match (Internet from 23-Aug-2016)
http://www.mdpi.com/1422-0067/13/8/10091/html

< 1% match (Internet from 10-Dec-2025)
https://www.mdpi.com/2073-4344/15/10/996

< 1% match (Internet from 21-Dec-2025)
https://www.mdpi.com/1420-3049/29/24/5954

< 1% match (Internet from 10-Dec-2025)
https://www.mdpi.com/1422-0067/26/13/6070

< 1% match (Internet from 10-Dec-2025)
https://www.mdpi.com/2079-6374/15/10/684

< 1% match (Internet from 13-Apr-2024)
https://WWW.MDPI.COM/1996-1944/16/17/5800

< 1% match (Internet from 10-Dec-2025)
https://www.mdpi.com/2073-4344/15/5/463

< 1% match (Internet from 12-Apr-2024)
https://www.mdpi.com/2304-8158/13/7/1116

< 1% match (Internet from 05-Jan-2026)
https://www.mdpi.com/1420-3049/30/18/3760

< 1% match (Internet from 10-Dec-2025)
https://www.mdpi.com/2073-4344/15/7/648

< 1% match (Internet from 10-Jun-2025)
https://www.mdpi.com/2073-4360/17/10/1331

< 1% match (Internet from 10-Dec-2025)
https://www.mdpi.com/2073-4360/17/7/953

< 1% match (Internet from 02-Feb-2024)
https://www.mdpi.com/2072-6694/15/3/6

< 1% match (Internet from 01-Jan-2026)
https://www.mdpi.com/2304-8158/13/5/810/xml

< 1% match (Internet from 28-Dec-2025)
https://www.mdpi.com/2073-4344/15/7/629/xml

< 1% match (Internet from 26-Dec-2025)
https://www.mdpi.com/1420-3049/27/19/6246/xml

< 1% match (Internet from 30-Dec-2025)
https://www.mdpi.com/2076-2607/13/2/303/xml

< 1% match (Internet from 24-Dec-2025)
https://www.mdpi.com/2079-4991/15/1/45/xml

< 1% match (Internet from 16-Feb-2025)
https://WWW.MDPI.COM/1420-3049/29/14/3397

< 1% match (Internet from 13-Mar-2025)
https://www.mdpi.com/2079-4991/15/5/365

< 1% match (Internet from 16-Dec-2025)
https://www.mdpi.com/2073-4344/15/12/1163